Theoretical and Experimental Research Studies of Full Vector, 3-D, Quantitative, Inverse Scattering, Ground Penetrating Radar

Final Report

David T. Borup
Steven A. Johnson
Michael J. Berggren
James W. Wiskin

TechniScan Inc.
825 N. 300 West
Suite 102
Salt Lake City, Utah 84103

July 2000

Contract F49620-95-C-0024, DEF

Prepared for

Air Force Office of Scientific Research
110 Duncan Avenue Suite B115
Bolling AFB DC 20332-0001

REPORT DOCUMENTATION PAGE

AFRL-SR-BL-TR-00-

0466

Public reporting burden for this collection of information is estimated to average 1 hour per response, existing data sources, gathering and maintaining the data needed, and completing and reviewing this cc burden estimate or any other aspect of this collection of information, including suggestions for reducing Headquarters Services, Directorate for Information Operations and Reports (0704-0188), 1215 Jefferson Respondents should be aware that notwithstanding any other provision of law, no person shall be subject information if it does not display a currently valid OMB control number. **PLEASE DO NOT RETURN YOUR FORM TO THE ABOVE ADDRESS.**

1. REPORT DATE *(DD-MM-YYYY)* 18-07-00	2. REPORT TYPE Final Technical Report	3. DATES COVERED *(From - To)* 01-03-95 to 01-03-98

4. TITLE AND SUBTITLE	
Theoretical and Experimental Research Studies of Full Vector, 3-D, Quantitative, Inverse Scattering, Ground Penetrating Radar	**5a. CONTRACT NUMBER** F94620-95-C-0024,DEF
	5b. GRANT NUMBER
	5c. PROGRAM ELEMENT NUMBER

6. AUTHOR(S) David T. Bourp, Steven A. Johnson, James W. Wiskin and Michael Berggren	
	5d. PROJECT NUMBER
	5e. TASK NUMBER
	5f. WORK UNIT NUMBER

7. PERFORMING ORGANIZATION NAME(S) AND ADDRESS(ES) TechniScan Inc. Northgate Business Center 350 West 800 North Suite 305 Salt Lake City, Utah 84103	8. PERFORMING ORGANIZATION REPORT NUMBER

9. SPONSORING / MONITORING AGENCY NAME(S) AND ADDRESS(ES) Air Force Office of Scientific Research 110 Duncan Avenue Suite Bolling AFB DC 20332-0001	10. SPONSOR/MONITOR'S ACRONYM(S) AFOSR
	11. SPONSOR/MONITOR'S REPORT NUMBER(S) 0002AA

12. DISTRIBUTION / AVAILABILITY STATEMENT

Unlimited

13. SUPPLEMENTARY NOTES

14. ABSTRACT

This final report describes the research work performed by TechniScan Inc. under Air Force Office of Scientific Research contract no. F94620-95-C-0024 for the period March 1, 1995 to March 1, 1998. The principal goal of the project was to advance the imaging capability of Ground Penetrating Radar (GPR) via the application of full wave, vector, 3D inverse scattering (IS) methods and to demonstrate the utility of this approach with a laboratory scale (1/20 th scale, 1-18 GHz) GPR scanner. Inverse scatter imaging of complex 3D targets was not achieved due to laboratory equipment limitations. Nonetheless, we believe that the theoretical advances, the software written, the simulations completed and the 2D practical laboratory demonstrations, provided by this research contract, taken together as a whole, constitute a remarkable, significant and valuable contribution to basic science, to engineering know-how and to technology. This body of new knowledge has the potential for application to many commercial areas.

15. SUBJECT TERMS

electromagnetic, ground penetrating radar, inverse scattering

16. SECURITY CLASSIFICATION OF:			17. LIMITATION OF ABSTRACT	18. NUMBER OF PAGES	19a. NAME OF RESPONSIBLE PERSON Steven A. Johnson
a. REPORT Unclassified	b. ABSTRACT Unclassified	c. THIS PAGE Unclassified	UL	34	19b. TELEPHONE NUMBER *(include area code)* 801-521-0888

Standard Form 298 (Rev. 8-98)
Prescribed by ANSI Std. Z39.18

Table of Contents

List of Symbols and Acronyms

Symbols:

$\rho = (x, y)$ 2-D coordinate vector

$|\rho|$ Magnitude of coordinate vector ρ

$\omega = 2\pi f$ Angular frequency where f is the frequency in cycles/sec.

ε_0 Permittivity of free space = 8.854×10^{-12} Farad / m.

μ_0 Permeability of free space = $4\pi \times 10^{-7}$ Henry / m.

$\varepsilon = (\varepsilon' - i\varepsilon'')$ Complex permittivity

$\mu = (\mu' - i\mu'')$ Complex permeability

ε^0 Real Debye permittivity at zero frequency

ε^∞ Real Debye permittivity at infinite frequency

τ Debye characteristic relaxation time

$\hat{y} = (\omega\varepsilon''(\omega) + i\omega\varepsilon'(\omega))$ Medium admittivity

$\hat{z} = (\omega\mu''(\omega) + i\omega\mu'(\omega))$ Medium impedivity

$\sigma = \omega\varepsilon_0\varepsilon''$ medium conductivity

γ Object scattering potential (typically $= \varepsilon / \varepsilon_0 - i\dfrac{\sigma}{\omega\varepsilon_0} - 1$)

c_0 Speed of wave propagation in air = 3×10^8 m/s

k_0 $= \omega/c_0$ Wave number in air

E   Electric field intensity vector

H   Magnetic field intensity vector

I   Identity operator

g_γ Green's function for object γ

g_0 Green's function for a whole space with wave number k_0

G_γ Green's function operator for object γ

G_0 Green's function operator for a whole space with wave number k_0

$\{A\}_{n',m'}^{n,m}$ Component of 2-D to 2-D discrete linear operator, A, for range point (n, m) and domain point (n', m')

Γ Operator corresponding to pointwise multiplication by γ.

Acronyms:

AFOSR	Air Force Office of Scientific Research
TSI	TechniScan Inc.
GPR	Ground penetrating radar
ISGPR	Inverse scattering, ground penetrating radar
GPISAR	Ground penetrating, imaging, synthetic aperture radar
FDTD	Finite- difference, time-domain method
IE	Integral equation
PML	Perfectly matched layer
BEM	Boundary Element Method
FFT	Fast Fourier Transform
IS	Inverse scattering
EM	Electromagnetic
TM	Transverse magnetic polarization
TE	Transverse electric polarization
1-D	One dimensional
2-D	Two dimensional
3-D	Three dimensional

1. Project Summary

This final report describes the research work performed by TechniScan Inc. (TSI) on Air Force Office of Scientific Research contract no. F94620-95-C-0024 for the period March 1, 1995 to March 1, 1998.

The principal goal of the project was to advance the imaging capability of Ground Penetrating Radar (GPR) via the application of full wave, vector, 3D inverse scattering (IS) methods. Conventional GPR systems display reflected energy versus time to provide a crude "reflector image" of the subsurface environment. Theoretically, inverse scattering methods provide a means of obtaining much more information from the reflected radar signals allowing for the quantitative (actual values of the electrical properties of the medium), registered and focused (removal of refraction and diffraction effects) imaging of the subsurface environment. However, the application of IS to GPR data requires much more from the GPR system. Specifically, IS requires very broad band data over a large aperture plus a detailed knowledge of the vector EM fields generated by the GPR system and antennas. In addition, antennas that are impedance matched to couple directly to the ground, rather than antennas designed to couple into air, are more difficult to manufacture and use, but would give images with higher spatial resolution (as much as 2 to 4 times better). The need to accurately characterize the fields generated by the GPR antennas is referred to as the *calibration problem*. In addition, the computational complexity of the inverse scattering algorithm must be reduced (compared with present implementations) to make a 3D vector GPR inverse scattering system practical.

TSI undertook this project in order to advance TSI scattering theory, inverse scattering algorithms and experimental/algorithmic calibration methods, developed primarily for the IS imaging of human tissue with ultrasound, to the electromagnetic GPR problem. TSI had already developed a laboratory scale GPR system from a contract through the Buried Waste Integrated Demonstration (BWID) program, managed by EG&G, Idaho, Inc., for the DOE at the DOE's Idaho National Engineering Laboratory, Idaho, Falls, Idaho. The purpose of the present AFSOR contract was to further advance TSI's theoretical, algorithmic and experimental methods and to provide a laboratory confirmation of the advantages and practicality of Inverse Scattering, Ground Penetrating Radar (ISGPR).

Unfortunately, some of TSI's original goals were not achieved. This was due mostly to the limited laboratory equipment available and a limited AFOSR budget that did not allow for extensive modifications to the laboratory scanner. In particular, it became evident that the original TSI x-y translation scanner and soil box were too small (6' by 4' and 16" deep for the sand box) to obtain the large aperture scattering data needed to image complex 2D objects. Also, since the antennas used were air-coupled horn antennas hovering above the surface of the sand box, Snell's law limited the effective scattering aperture to $\pm 30°$ for buried targets, severely restricting the lateral (direction normal to depth for 2D) resolution of the system. This, coupled with large signal reflection losses at the air-sand interface and clutter signals form the scanner frame and sand box sides and bottom, made the imaging of general 2D objects unworkable. TSI's original goal of 2D and 3D reconstructions of complex targets in the laboratory was successful for 2D targets, but 3D targets were imaged only as multipley 2D slices by applying the 2D imagaing method to data from multiple 2D slice scans. TSI's best inverse scattering reconstruction is of a circular cylinder buried in the sand and imaged with a circular symmetry constraint (which effectively fills out the missing lateral scan data).

TSI has concluded that further development of ISGPR will require a larger data acquisition and scanning apparatus (to give an optimally large "numerical aperture" in the theory of optics sense) and broad band, earth-coupled antennas that are placed in direct contact with the soil (to avoid the Snell's law limitation). The cost to have such antennas designed and built at 1/10 th scale laboratory frequencies (1-20 GHz) is in excess of $100K. Since full scale field antennas (100 MHz to 3 GHz) which are already available cost about the same price, TSI has concluded that the next logical step is to procure funding to build a full scale field system. This system would initially be calibrated and tested in a large, environmentally controlled soil pit (located in a warehouse, for example). TSI is presently preparing a proposal to the DOE to construct this system. The theoretical, algorithmic and experimental results achieved during the performance of this AFOSR contract substantially advanced the understanding of ISGPR and have effectively paved the way for the DOE field system.

The specific objectives of the proposed research are described in the next section. Many of the results from this contract were published in the papers cited in section 4 of this report.

2. Objectives of the Research

The objectives originally proposed by TechniScan (TSI) and funded by the AFOSR are listed below. Following each objective is a brief statement of the progress made for that objective during the contract period.

Objective a. Generalize existing 2-D acoustic transducer equivalent source optimization theory for electromagnetic (EM) modeling for 2-D vector and 3-D vector equivalent sources. Write algorithms to be implemented for EM-type imaging applications and then test with simulated data. Conduct 2-D and 3-D laboratory-scale tests to collect data to generate optimized equivalent source antenna models.

Progress made on objective a. TSI's 2D acoustic equivalent source optimization method was generalized to model a 3D aperture antenna by an equivalent tangential, vector magnetic current sheet. Laboratory data for TSI's 1-18 GHz, ridged microwave horn antennas were collected for the purpose of optimizing this current sheet to match these data, thereby calibrating the antennas in the most general sense (3D vector field calibration). However, simulations with 3D apertures and evidence from laboratory data convinced TSI that simple scalar (TM polarization) models of the antennas are effective for 2D targets buried in the laboratory sand box. Since TSI did not get to the 3D target case (with the exception of our Ground Penetrating, Imaging, Synthetic Aperture Radar (GPISAR) experiments) we did not complete development of the full vector 3D calibration method.

Objective b. Extend 2-D scalar EM analytical scattering solutions to 2-D vector, 2.5-D vector, and 3-D vector analytical scattering solutions for objects buried in a half-space. Encode in forward model and incorporate optimized antenna models. Conduct 2-D and 3-D tests on objects in air and compare with simulations.

Progress made on objective b. Two exact EM codes for canonical objects were developed. The first is a 2.5D vector code which computes exact scattering of a general 3D vector EM wave from a layered cylinder. The second code computes scattering from a layered sphere from a magnetic current element with arbitrary orientation. Since any aperture EM source can be modeled with an equivalent, tangential magnetic current on a plane, this code can compute layered sphere scattering from any aperture antenna. Because our laboratory work concentrated on 2D test objects illuminated with the TM polarization (a case which was found to be accurately modeled by 2D scalar theory) these codes were not used on experimental data. They will, however, be essential for the calibration of 3D vector data collected by future TSI GPR scanners.

Objective c. Develop theory that incorporates causality constraints in dispersive media.

Progress made on objective c. In the first year of the contract, a novel theory for the inversion for the Debye parameters of a single relaxation material was derived. This theory is detailed in Appendix B of TechniScan Inc.'s First year Technical Report. In the second year of the contract, a novel Finite Difference, Time Domain (FDTD) algorithm was derived and programmed which incorporates a multiple pole, Debye model for dispersion. This work was published in publication 4.2 cited in section 4 of this report.

Objective d. Extend 2-D and 3-D image inversion codes to include optimized antenna models and causally dispersive media models. Investigate the role of multiple polarization data and causality constraints. Examine the range of applicability of the 2-D inversion problem. Conduct laboratory-scale experiments to collect data on objects buried in characterized soils and compare with simulations.

Progress made on objective d. TSI did develop 2D and 3D vector EM inverse scattering codes which can make use of optimized antenna models, however, due to the limitations of the experimental equipment described in section 1. above, they were never applied to laboratory data. TSI's work on causality constraints applied to inverse scattering is discussed in the objective c above.

Objective e. Develop 2-D and 3-D imaging theory and algorithms using surface integral equation models for scattering from impenetrable and high contrast materials.

Progress made on objective e. During the first year, the boundary element method (BEM) was investigated (see Appendix E of TechniScan Inc.'s First year Technical Report). This frequency domain, surface integral equation approach is limited in its applicability to the GPR problem because the GPR problem often involves both penetrable (volumetric) and impenetrable (surface) targets. The generalization of the BEM to incorporate inhomogeneous, volumetric scatterers, via coupling to an volumetric integral equation formulation for the penetrable part, would be difficult. Instead, TSI focused its efforts on the development of a finite difference, time

domain inverse scattering algorithm which can model both penetrable and impenetrable targets. This method has been programmed and tested for penetrable targets. Future work by TSI will generalize this algorithm for the mixed penetrable/impenetrable case.

Objective f. Examine the stability of the cylindrical coordinate recursion algorithm and test methods to precondition the forward and inverse problems.

Progress made on objective f. The cylindrical coordinate recursion method (CCR) is an approach originally derived by TSI for transmission mode (data collected on the side of the object opposite the transmitter) imaging. Due to the cylindrical coordinate basis of the CCR and the natural rectangular nature of the GPR problem (vertical stratification) we determined that this approach is not well suited for GPR. Instead, we concentrated on the problem of preconditioning the TSI integral equation (IE) approach which can directly model vertical stratification via use of the layered Green's function. TSI found a novel and very powerful preconditioner for the special case of a homogeneous target. This preconditioner was demonstrated to increase the convergence rate of the IE iterative solution by as much as a factor of ten! In fact, the preconditioned method converges for cases where the unpreconditioned IE method fails to converge at all. The method was also shown to be effective for the 2D vector TE polarization which is a strong indication that it will work for the 3D vector case as well. Unfortunately, a generalization of the preconditioner for a nonhomogeneous object has not yet been found. Further work on this preconditioning method will be necessary to resolve this limitation. TSI feels that this approach will play a significant role in the future application of inverse scattering to GPR imaging. Appendix C of TechniScan Inc.'s First year Technical Report describes the theory and implementation of this preconditioner in detail.

Objective g. Extend theory of scattering to include presence of magnetic materials. Extend algorithms to incorporate this effect. Conduct laboratory-scale tests on objects buried in characterized soil with magnetic properties. Compare test data to forward and inverse simulations. Investigate the ill-posedness of simultaneous inversion of $\hat{y}$ and $\hat{z}$ terms.

Progress made on objective g. In the first year of the contract, a novel theory for the simultaneous inversion for electric and magnetic material parameters from EM scattering data was derived. This theory is detailed in Appendix D of TechniScan Inc.'s First year Technical Report. While a full analysis of the illposedness of the simultaneous inversion for the $\hat{y}$ and $\hat{z}$ terms was not performed, the data transform derived in Appendix D theoretically improves the conditioning of this separation a great deal.. We did not do any laboratory experiments with magnetic materials.

3.   Research Results

In the next four sections, the accomplishments and results for each of the four reporting periods (3/95-3/96, 3/96-9/96, 9/96-9/97, and 9/97-3/98) is summarized with detailed results given for the last, previously unreported, period.

3.1   Research Results from 3-95 to 3-96

The results for this year are detailed in TechniScan Inc.'s First year Technical Report sent to the AFOSR on 4/96. The following is a brief summary of the main accomplishments and results.

In the first year of the project, TSI made extensive modifications to the laboratory scale GPR scanner and control hardware and software. The soil box was placed on slotted wheels that slide on metal rails, allowing the soil box to be smoothly slid out from under the scanner. This allowed easy placement and removal of buried test objects without disturbing the system calibration. The motor and network analyzer control software was reprogrammed in LabView$_{TM}$; LabView$_{TM}$ being an object oriented environment for experiment control and data collection, which runs in Windows 95 on the control computer. This greatly eased the reprogramming of the motor scan pattern and network analyzer set up. Figure 3.1.1 shows the x-y translation scanner after modification.

Calibration data for TSI's 1-18 GHz ridged horn antennas were collected. The calibration code for using this data to create equivalent magnetic current models of the 1-18 GHz ridged horn antennas was developed but not tested on lab data.

The exact solution of a circular cylinder buried in a half space, illuminated by a 3-D vector field from an arbitrary antenna in the air above the half space was formulated. The purpose of this code was to refine and confirm the

accuracy of the laboratory antenna calibrations by comparison of the simulation with data collected in the laboratory.

A Boundary Element Method (BEM) algorithm for forward scattering of 2-D Transverse Magnetic (TM) waves was written. The purpose of this code was to simulate scattering from buried high dielectric contrast materials and metallic surfaces. Appendix E of TechniScan Inc.'s First year Technical Report details the BEM algorithm.

TSI began the analysis of causally dispersive media by examining the Debye formulation for single relaxation dispersion. A novel inverse scattering approach for the imaging of Debye parameters in 1-D was developed. Details of the approach were included in Appendix B of TechniScan Inc.'s First year Technical Report. A number of numerical tools were developed including analytic solutions in 1-D, and a finite-difference, time-domain (FDTD) algorithm with perfectly matched layer (PML) boundary conditions and Debye dispersion in 1-D and 2-D. Details on the implementation of the non-dispersive PML boundary condition for the 2-D acoustic case (equivalent to the 2-D TM polarized EM case) was included as Appendix A of TechniScan Inc.'s First year Technical Report and was published in publication 4.1 cited in section 4 of this report.

A novel theory for the simultaneous inversion of electrical and magnetic properties in 2-D with TM polarized waves was developed and included as Appendix D of TechniScan Inc.'s First year Technical Report.

A novel technique for preconditioning the 2-D TM scattering integral equation was developed. Simulation studies showed that this preconditioner accelerates the convergence rate of the iterative solution of the integral equation by a factor of 10 or more, particularly for the high dielectric contrasts encountered in the earth. In fact, high contrast problems that did not converge without the preconditioner were found to be rapidly convergent after preconditioning. Unfortunately, this preconditioner's formulation is applicable to homogeneous bodies only. A detailed analysis of this preconditioner and a proposed extension to inhomogeneous bodies was included in Appendix C of TechniScan Inc.'s First year Technical Report.

Images of 2-D and 3-D metallic objects buried in sand were made using TSI's Ground Penetrating Imaging Synthetic Aperture Radar (GPISAR) algorithm. This approach is not inverse scattering (the primary objective of this research) but is does give high-resolution images of reflectors. It turns out that this approach has had a high payoff with its application to an important NDT problem presented to TSI by a solid rocket motor manufacturer (see section 5.1 of this report).

A quantitative inverse scattering image of a 1-D layered structure consisting of dry wall board and sand was made from laboratory data. A better 1-D imaging result is shown in the next section.

3.2 Research Results from 3-96 to 9-96

The results for this period are detailed in TechniScan Inc.'s Second year Technical Report sent to the AFOSR on 10/96. The following is a brief summary of the main accomplishments and results.

The exact solution to the scattering problem of a multilayered sphere illuminated by an arbitrarily polarized element of magnetic current was formulated. The solution was realized in computer code and the results were checked using an integral equation solver and by comparison with the low frequency asymptotic solution. The ultimate purpose of this program is to model a buried sphere illuminated by an arbitrary antenna. Because any radiating aperture can be modeled by an equivalent 2-D magnetic surface current, we can expand any radiating aperture in terms of a linear combination of magnetic current elements.

A generalization of the 2-D scalar integral equation preconditioner (developed during year 1), using the incomplete LU factorization approach suggested in Appendix C of the first year report, was tested. This approach only achieved a factor of two speed-up. In the first year report, TSI showed cases where a speed up of a factor of 10 or more was obtained for the special case of a homogeneous body. TSI has yet to find an adequate generalization of this preconditioner for a general, inhomogeneous object.

TSI generalized the previously described perfectly matched layer (PML) FDTD algorithm is three important ways.

1. The second order spatial derivative approximation was replaced with a fourth order approximation. This modification allowed the spatial sample rate at the highest frequency to be increased from $\lambda/12$ (second order case) to $\lambda/6$ (fourth order case). In 3-D, this accelerates the solution speed for a given problem by a factor of 8! The fourth order scheme also reduces the computer storage by a factor of 8 over the second order scheme.

2. TSI generalized the PML-FDTD code to incorporate causally dispersive media models. These models are constructed by assuming a multiple pole Debye model of the dielectric. The details of this approach for the scalar wave equation (acoustic case) were given in Appendix A of TechniScan Inc.'s Second year Technical Report and was published in publication 4.2 cited in section 4 of this report.

3. TSI derived and programmed the PML FDTD algorithm with Debye dielectric models for the 2-D vector electromagnetic case (TE polarization). Appendix B of TechniScan Inc.'s Second year Technical Report describes this formulation in detail.

TSI constructed a new goneometer (angle scanner) for the collection of data for 1-D inverse scatter profiling of layered dielectric earth models. Figure 3.2.1 is a photo of the goneometer. The blue surface toward the bottom of the photo is a sheet of 2" thick Styrofoam lying on top of the sand in our 4' by 6' sandbox. The two 1-18 GHz, ridged horn antennas are mounted on two, three sided brackets of fiberglass which form the rotation arms of the goneometer. A bearing at each end of the sandbox forms the rotation axis. Also seen in Figure 3.2.1 is the HP 8720 network analyzer, which acts as the microwave source and receiver. A computer controlled motor and cable spindle lowers the two antennas in angle via steel cables that run along a centerboard (above the antennas). This scanner allows the collection of scattering data at multiple angles of incidence for 1-D layered slabs of material placed on the sand surface.

In order to test TSI's 1-D inverse scattering algorithms on real data, TSI used the goneometer scanner to collect data from some simple layered media. Figure 3.2.2 is a drawing that shows the geometry for a 1" layer of drywall followed by a 2" layer of polystyrene foam on top of the 15.5" thick sand layer in our sandbox.

Figure 3.2.3 shows the time domain comparison between the collected data and 1-D scattering theory. The theory assumes that ε_r(drywall)=2, ε_r(foam)=1 and ε_r(sand)=2.3. Since all of the materials are essentially lossless, the inversion TSI applied used a "realness" constraint on the dielectric constant for the inversion. Figure 3.2.4 compares the reconstructed image of ε_r-1 with the true value. The reconstruction is quite good, particularly in locating the positions of the dielectric interfaces. These results were published in the paper cited in reference 4.5 in section 4 of this report.

TSI performed several more GPISAR imaging experiments during the second year. Figure 3.2.5 shows the geometry of the x-y scanner used to collect the data.

The TSI soil box is 4' by 6' by 15.5" deep and filled with sand. For the following images, both antennas (1-18 GHz horns) were placed on the same x-y translator above the sandbox. Thus, the data collected are of the common offset data type (the transmitter and receiver are fixed relative to each other). Moving the transmitter performed a square scan of 60 by 60 cm in the x-y plane / receiver to 31 by 31 positions with a scan increment of 2 cm. The horn antenna feeds were 50 cm above the sand surface (in z).

Figure 3.2.6 shows a GPISAR image of a metal carpenter's square that was buried at a depth of about 6 inches. Figure 3.2.7 shows a GPISAR image of a metal caliper that was also buried at a depth of about 6 inches.

3.3   Research Results from 9-96 to 9-97

The results for this year are detailed in TechniScan Inc.'s Third year Progress Report sent to the AFOSR on 10/97. The following is a brief summary of the main accomplishments and results.

The first goal, which must be achieved in order to apply inverse scatter imaging, is the solution to the *calibration problem*. This refers to the requirement that the characteristics of the antenna fields in both space and time be known to sufficient accuracy. A model of these fields is then supplied to the imaging algorithm such that the scattering predictions of the algorithm match the collected data for a given target.

TSI's main effort for this period was aimed at improving the methodology with which the laboratory GPR scanner data is calibrated to the theory employed by the inversion algorithm. Refinement of this procedure resulted in a reasonable degree of match between theory and experiment. TSI was able to image the dielectric cross section of a 4", air-filled PVC pipe scanned with the x-y translation scanner using the 1-18 GHz horn antennas.

3.3.1 Development of an algorithm for data calibration via optimization

In order to match the buried, air-filled, PVC pipe laboratory GPR data to the theoretical predictions of the exact halfspace solution, accurate values of the dielectric constants (sand and plastic), burial depth, and other physical

parameters must be determined. For this purpose, an optimization algorithm was written which varies these parameters in the exact solution algorithm until the best match to the laboratory data is obtained. Figure 3.3.1 shows the best time domain match obtained to date for the PVC pipe signal. Figure 3.3.2 compares the exact solution and laboratory data in the frequency domain.

3.3.2 Inverse scatter imaging with a frequency domain, integral equation method

The frequency domain data were then inverted using a frequency domain, integral equation inversion algorithm. At the present time, data have been collected for only one view (transmitter/receiver antenna position). This, of course, is insufficient data to image a generic 2-D object. However, these data are sufficient to invert for the radial variation of a cylindrically symmetric object. In order to test the calibration of the data for this one view, a cylindrical symmetry constraint was incorporated into the inversion algorithm. Figure 3.3.3 shows the obtained reconstruction compared with the true dielectric distribution.

The bandwidth used in the reconstruction was 1 to 9 GHz. The reconstruction is fairly accurate and the plastic wall of the pipe is clearly detected, however the values outside of the pipe seem to be biased (gamma should be zero outside of the target). This is due to the fairly poor match between the data and theory for low temporal frequencies (see Figure 3.3.2). Also, the algorithm was unable to invert frequencies above 9 to 10 GHz. The reason for this has to do with the nature of the frequency domain, integral equation algorithm used. This algorithm solves the scattering problem via an iterative method. For the size and contrast (dielectric contrast) of the air-filled, PVC pipe, this iteration becomes very slow as the frequency is increased. Attempts were made to alleviate this problem by preconditioning of the iteration (see our year 1 and 2 reports). This was effective for some test objects but it did not adequately precondition the scattering algorithm for the inversion of the PVC pipe for frequencies above 9 GHz.

3.3.3 Development of a Finite Difference, Time Domain (FDTD) imaging algorithm

The convergence problems encountered for the frequency domain, integral equation approach can be remedied by reformulating the inverse problem in the time domain and using the Finite Difference, Time Domain (FDTD) algorithm to solve the scattering problems. For the broad band reflection mode case, this approach has advantages over the integral equation approach since all frequencies are computed with one time domain solution. In addition, the FDTD algorithm can model scattering from impenetrable (metallic) objects, which cannot be modeled by the volumetric integral equation methods. For these reasons, TSI has put extensive effort into coding an FDTD imaging algorithm. The method has the following features:

1. Fictitious boundary reflections from the FDTD grid boundary are alleviated by the use of the perfectly matched layer (PML) boundary condition (see our previous year 1 and year 2 reports for our contributions to this formulation).

2. The differencing scheme is 4th order in space, allowing a larger spatial sampling interval ($\lambda/6$ at the maximum frequency).

3. The algorithm does not need to compute outside of the target region. The transmitters and receivers that lie outside of the FDTD space are incorporated by Green's theorem.

This code was completed and tested during the final research period.

3.4 Research Results from 9-97 to 3-98

The results for this period are not discussed in previous reports and are thus described in detail.

3.4.1 Completion of development of a Finite Difference, Time Domain (FDTD) imaging algorithm

The FDTD imaging code was completed and tested in simulation. This approach has several advantages over the frequency domain, integral equation approach that TSI has used in the past. In particular, the calculation of the scattering from a target is not dependent on the convergence of an iterative method, but rather, is a finite step process (finite duration recurrence) and, thus, it can be applied to high contrast targets. Also, the FDTD method can be applied to problems that contain mixed penetrable and impenetrable (metallic) targets. TSI's implementation of the FDTD inverse scattering algorithm has the additional advantage of using a "pillbox" formulation. This means that the source and receiver antennas are incorporated by the application of Green's theorem at the FDTD boundary and, thus, the FDTD grid need only enclose the targets to be imaged - not the

entire space including the antennas (as with most other implementations). Future development of inverse scattering GPR by TSI will rely on this approach **and** the frequency domain integral equation approach - once a suitable preconditioner for the general, inhomogeneous body is found.

3.4.2 TE preconditioning

The previously reported preconditioner for the TM polarization and a homogeneous target was derived and tested for the TE polarization. The resulting preconditioning effect was as significant - a factor of 10 speed up in the convergence rate - as for the TM case. This suggests that the preconditioner will perform well for the 3D-vector case for homogeneous bodies. Further research on methods to apply this technique to inhomogeneous bodies is needed and likely to have a major impact on the applicability to inverse scattering to GPR imaging.

3.4.3 Transmission mode imaging of dielectric targets

Prior to and concurrent with the AFOSR contract, TSI was involved in the "Sea Ice Project" funded by the Office of Naval Research under contracts N00014-93-10141 and N00014-94-10958. The broad aim of the project was to advance the theoretical and empirical understanding of the electromagnetic properties of sea ice. TSI's main focus was to develop a laboratory data acquisition system and inverse scattering algorithms for the imaging and characterization of ice samples. The theoretical and experimental similarity of the Sea Ice Project with TSI's AFOSR project naturally led to a great deal of synergy - both projects receiving substantial benefit from the other. Although TSI was not originally contracted to collect broad band, reflection mode data for the Sea Ice Project, the equipment procured for the AFOSR project (HP network analyzer and Ridged horn antennas) allowed TSI to provide the Sea Ice Project researchers with the accurately calibrated reflection data described in section 3.2 of this report. In fact, the only laboratory data successfully inverted by TSI and the other Sea Ice researchers came from the TSI laboratory. A complete description of the Sea Ice Project results was published in the paper cited in reference 4.5 in section 4 of this report.

During the initial phase of TSI's work on the Sea Ice Project a x-band EM tomographic scanner was constructed. The scanner consisted of two computer controlled rotation stages, allowing a x-band horn, receiving antenna to be rotated from $-150°$ to $150°$ (relative to the transmitting horn). The second rotation stage allowed the test object to be rotated for the collection of multiple view data. This scanner was constructed mostly of wood and was not sufficiently ridged to provide precise position control.

As an example of our early imaging efforts, Figure 3.4.1 shows a reconstruction of a 6" by 4" wooden block. Data were taken for 30 view angles at a frequency of 10 GHz. Although our imaging algorithm was able to delineate the shape fairly well, there are clearly artifacts in the image. In addition, the imaging algorithm gave real and imaginary parts of γ that were roughly equal in magnitude (the figure is the magnitude of the complex γ).

Since the wood was very dry, the imaginary part γ should have been very small. This is a typical result when inverse scattering is applied to un-calibrated data. Phase inaccuracies in the data due to uncertainty in the geometrical alignment of the scanner cause a mixing of the real and imaginary parts (a phase shift) in the image. As a result, the imaging algorithm did not give an accurate, quantitative reconstruction of the dielectric parameters of the wood.

Results like Figure 3.4.1 convinced us that the geometrical parameters of the scanner needed to be more accurately measured or calibrated for in the software and that the scanner needed to be much more stable mechanically. These considerations motivated the construction of the scanner shown in Figure 3.4.2.

The transmitter x-band horn antenna (10 GHz) is seen on the left and is fixed. The receiver x-band horn antenna is seen on the right. Both the movable receiver horn and the object rotate about a common center of rotation. Each is mounted on a stepping motor driven rotation stage. The receiver stage rotates about the fixed transmitter. The object stage is mounted coaxially on the receiver stage and rotates about the receiver. The receiver horn coaxial cable is coupled to a rotating coaxial feed-through coupler. A Hewlett Packard network analyzer drives the transmitter horn and receives signals from the receiver horn. A Pentium computer controls the stepping motors and the network analyzer and stores data to be sent over the internet to a workstation for inverse imaging. The large rotation stage at the bottom moves the receiver horn. The target shown is a plastic pipe.

In order to accurately match our experimental scattering measurements to our inversion algorithms, TSI has developed a calibration method to determine several physical parameters of the measurement system. The method uses experimental data from a simple shape with a known scattering solution - a multilayered, circular cylinder - to

determine the calibration parameters by an optimization algorithm. The calibration parameters include various geometrical offsets in the scanner and the electrical parameters of the calibration target. Figure 3.4.3 shows the calibration parameters for this case.

The parameters to be determined by the calibration algorithm are:

ρ_t = the distance from the transmitter horn face to the center of the receiver rotation axis

ρ_r = the distance from the receiver horn face to the center of the receiver rotation axis

α_t = the angle offset of the transmitter horn

α_r = the angle offset of the receiver horn

ϕ_s = the angle of the receiver for the first receiver position

$Re(\varepsilon_r)$ of each layer of the target

$Im(\varepsilon_r)$ of each layer of the target

δ_x = the x offset of the target center

δ_y = the y offset of the target center

The first five parameters define the geometrical offsets of the scanner. The other parameters define the target and its placement relative to the receiver horn axis of rotation. To illustrate this method, consider the following example: a PVC pipe with a 22-cm outer diameter and a 19-cm inner diameter was placed at the center of the receiver rotation. Both the receiver and transmitter horn faces were about 36 cm from the receiver rotation axis.

Data were then taken at 10 GHz for the receiver rotated from −150° to 150° with a step of 2° (151 receiver positions). Data were taken and without the PVC pipe present (total and incident field measurements). An initial guess for the calibration parameters was obtained by careful physical alignment of the scanning system followed by measurement of the important geometrical parameters (e.g., the distances of the horns from the receiver rotation axis, etc.) For this initial guess of the calibration parameters the simulated data was generated. The lab data and the simulation are compared in Figures 3.4.4 and 3.4.5. The initial data/theory mismatch is 53 %. After application of TSI's calibration algorithm this error was reduced to 9%. The match between the data and the calibrated simulation is shown in Figures 3.4.6 and 3.4.7. Note the great improvement in the data/theory match over the uncalibrated data (Figures 3.4.4 and 3.4.5.). In particular, the phase match, Figures 3.4.7 is extremely good. Some of the error that is present, particularly in the magnitude match, may be due to out of plane misalignments of the experiment that cannot be accounted for with a 2D-calibration algorithm. Another possible source of error is the fact that the calibration algorithms (and our inversion algorithms) assume a 2D TM scalar field model while the true horn fields are 3D vectors.

Once the calibration parameters have been found, they are incorporated into the inverse scattering algorithm. Figures 3.4.8 and 3.4.9 show the result of applying our inverse scattering algorithm to the calibrated data. For this case a 60 by 60, $\lambda_0/6$ array was used to discretize the inverse problem. The figures show the true and reconstructed real and imaginary parts of γ on the x-axis through the center of the PVC pipe. Note that the reconstruction of the real part of γ is not too bad, however the imaginary part is quite poor. In particular, the imaginary part, which **must** be negative, oscillates significantly and has many positive values. Because the imaginary part of the plastic is very small relative to the real part (−0.06 compared with 1.8) the quantitative imaging of the imaginary part is very difficult. In order to remedy this problem, TSI has developed an inversion algorithm that constrains the real part of γ to be positive (which must be true if the target is in air) and the imaginary part to be negative by the simple change of variables:

$$\gamma(x,y) = \alpha^2 - i\beta^2$$

This algorithm was applied to the data using a 120 by 120, $\lambda_0/12$ pixel array. Figures 3.4.10 and 3.4.11 show the result. Notice the much greater agreement between the true and reconstructed object both in the real and imaginary parts. This is especially remarkable since inverse scattering theory suggests that the target cannot be reconstructed at a resolution greater than $\lambda/4$ where λ is the wavelength in the target (λ = about $\lambda_0/1.5$ for plastic).

Note also that the imaginary part is now quite quantitatively accurate. Clearly, the constraint is very powerful, providing much greater quantitative accuracy and a degree of super resolution for this case.

A problem yet to be solved is seen in the reconstruction shown in Figure 3.4.10. Notice that the walls of the tube are very accurately reconstructed, however, a dip in the reconstruction occurs inside the plastic. It turns out that, in fact, the solution shown in Figure 3.4.10 is a local minimum. We have verified this by starting the inverse scattering iteration with the true solution (the solid lines in Figures 3.4.10 and 3.4.11). When this is done, the iterates stay very close to the true solution and never develop this dip. We have also seen this local minimum problem for solid rods of plastic. This occurs even when the starting guess for the inversion has a phase shift equal to the true object (for example, when the algorithm starts with a smoothed version of the true solution). This occurs for both simulated and laboratory data whenever the contrast of the target is large. This local minimum problem does not occur for low contrast objects, even when they are large in size. We believe that for high contrast materials, the overdetermined Jacobian of the nonlinear system becomes row rank deficient as the computed internal fields deviate significantly from the incident fields. The original notion that one frequency is sufficient in the transmission mode tomographic reconstruction problem is based on an analysis of the Born approximation for which the internal fields are assumed to deviate only weakly from the incident fields. In this case, one can prove that the Jacobian has complete row rank (to within the resolution of the illuminating wavelength) if the angular coverage is complete (transmitters and receivers all the way around the target). It now appears that this is not the case for high contrast materials for which the internal fields deviate greatly from the incident wave (and for which strong reflections occur). One obvious way to attempt to complete the rank of the Jacobian is to add multiple frequencies. In fact, we know from our reflection imaging work that this works. We have imaged high contrast objects in reflection mode using full bandwidth data in both simulation and in the laboratory and do not observe this problem. The difficulty of this solution for the transmission mode tomographic problem is that typical scanners utilize a simple horn antenna with limited bandwidth capability. For example, the horns on our tomographic scanner are x-band horns with a usable bandwidth of 8-12 GHz. Unfortunately, the data collected for the above example was single frequency data and we have yet to determine what bandwidth is needed to avoid the local minimum. TSI plans to further investigate this problem with both simulated and laboratory data to determine the bandwidth requirements as a function of size and contrast. To our knowledge, no other group working in this field is yet aware of this problem due to the unavailability of well-calibrated data. These results were presented in the invited lecture cited in reference 4.6 in section 4 of this report.

3.4.4 Development of a vector EM, Finite Difference, Time Domain (FDTD) scattering algorithm for dispersive media

This method was published in the paper cited in reference 4.3 in section 4 in this report.

4.   Papers Published

4.1 Yuan, X. ,Wiskin, J. W., D. T. Borup, M. Berggren, R. Eidens, S. A. Johnson, "Formulation and Validation of Berenger's PML Absorbing Boundary for the FDTD simulation of Acoustic Scattering", *IEEE Trans. UFFC. 44, 4, 1997 (IEEE Trans Ultrason., Ferro, Freq. Control.)*

4.2 Yuan, X., D. Borup D. T., Wiskin, J. W., Berggren, M., Johnson, S. A. and R. Eidens, "Simulation of acoustic wave propagation in dispersive media with relaxation losses by using FDTD methods with PML absorbing boundary condition", *I.E.E.E. Trans. of Ultrasonics, Ferro., and Freq. Control.*, **46**, No. 1, January, 1999.

4.3 Yuan:, X., D. Borup D. T., Wiskin, J. W., Berggren, M., Johnson, S. A, "Extension of The PML Absorbing Boundary Condition to FDTD Simulation of EM Wave Propagation in Dispersive Media," submitted to *IEEE Trans. Antennas Propagat.*

4.4 Johnson, S. A., David T. Borup, James W. Wiskin, Michael J. Berggren, Michael S. Zhdanov, Kyle Bunch, and Richard Eidens, "Application of Inverse Scattering and Other Refraction Corrected methods to Environmental Imaging with Acoustic or Electromagnetic Energy", in *Next Generation Environmental models and computational methods., Ed. George Delic, Mary F. Wheeler,* Proceedings of a U.S. Environmental Protection Agency sponsored workshop at the National Environmental Supercomputing Center, S.I.A.M., 1997.

4.5 Golden, K. M., Borup, D., Cheney, M., Cherkaeva, E., Dawson, M.S., Ding, K.H., Fung, A.K., Isaacson, D., Johnson S.A., Jordan, A.K., Kong, J. A., Kwok, R., Nghiem, S.V., Onstott, R.G., Sylvester, J., Winebrenner, D.P., and Zabel, I.H.H.,"Inverse Electromagnetic Scattering Models for Sea Ice", *IEEE Trans. Geosci. and Rem. Sens.*, **36,** No.5, p. 1675, 1998.

4.6 "Integrating Experimental Procedures with Algorithms for Practical Imaging by Full Wave, Non-Linear Inverse Scattering," *Invited Lecture, Assemblee' Ge'ne'rale de l'Union radio-scientifique internationale, XXVIth General Assembly of the International Union of Radio Science (U.R.S.I.), Aug. 13-21, 1999,* Toronto, Ontario, Canada.

5.   Applications of the Developed Technology

Other TSI research projects directly aided and advanced by the AFOSR project results:

5.1 Sea Ice Project

Prior to and concurrent with the AFOSR GPR contract, TSI was involved in the "Sea Ice Project" funded by the Office of Naval Research under contracts N00014-93-10141 and N00014-94-10958. The broad aim of the project was to form and use of a consortium of high level research groups from universities and research institutions to advance the theoretical and empirical understanding of the electromagnetic (RF to optical) properties of sea ice. TSI's main focus was to: (1) develop a laboratory data acquisition system for use by TechniScan and other members of the consortium; (2) develop an inverse scattering algorithms for the imaging and characterization of ice samples; and (3) to apply the TechniScan imaging algorithms to data collected on the TechniScan scanner. The theoretical and experimental similarity of the Sea Ice Project with TSI's AFOSR project naturally led to a great deal of synergy - both projects receiving substantial benefit from the other. Although TSI was not originally contracted to collect broad band, reflection mode data for the Sea Ice Project, the equipment procured for the AFOSR project (HP network analyzer and Ridged horn antennas) allowed TSI to provide the Sea Ice Project researchers with the accurately calibrated reflection data described in section 3.2 of this report. In fact, the only laboratory data successfully inverted by TSI and the other Sea Ice consortium researchers came from the TSI laboratory. A complete description of this particular Sea Ice Project results (and related projects) was published in a special issue of the IEEE Trans. Geosci. and Rem. Sens., which includes the paper cited in reference 4.5 in section 4 of this report.

5.2 GPISAR algorithms applied to rocket motor imaging.

An important spin-off application of the work performed by TSI for this contract concerned an NDT problem that a major solid fuel rocket motor manufacturer contracted TSI to solve (this rocket motor manufacturer, hereafter referred to as the "customer" wishes to remain anonymous). The problem arose from the possibility that a set of three foreign objects may have fallen into the fuel mixer prior to the fuel loading and casting process of four rocket motor sections. Simulations of the conditions in the rocket motors during flight indicated that the presence of these foreign objects might result in a significant change in the burn profile or even a catastrophic failure. The customer contracted TSI to aid in the analysis of microwave and acoustic scattering data from both fuel defect standards (blocks of fuel cast with and without the foreign objects present) and from the rocket motor sections in order to aid in assessing whether or not the rocket motors should be launched. These rocket motor sections represented a $20 million dollar investment by the customer.

Initial simulation work by TSI and experimental work by the customer indicated that the electromagnetic loss of the fuel was too high for microwave detection of the foreign objects to a sufficient depth in the fuel and so the research focused on the acoustic detection option. Simulations by TSI and experimental work by the customer refined the design and final configuration of the scanner to the apparatus shown in Figure 5.2.1.

The scanner consists of two, 1" diameter disk transducers (one transmitter and one receiver separated center to center by slightly more than 1 inch) with a center frequency of 280 KHz. Acoustic coupling to the fuel is maintained by a flow of Flourinert^{TM} fluid. The transducers are scanned across the fuel surface by a set of computer controlled stepping motors. The object being scanned in Figure 5.2.1 is one of the fuel defect standards.

Figure 5.2.2 compares an unfocused C-scan image - the approach originally developed by the customer - and a focused, synthetic aperture C-scan image generated by the algorithm developed by TSI for a fuel defect standard containing an embedded rubber defect.

The plane of the images in Figure 5.2.1 is parallel to the plane of the fuel surface. Notice that the original customer algorithm is unable to discriminate the rubber defects from the numerous air voids that occur in the fuel; however, the TSI focused, synthetic aperture algorithm very clearly reproduces the rubber defect shapes. Also, the air void resolution is much greater and their round shape easily distinguishes them. The focused, synthetic aperture algorithm supplied to the customer by TSI is, in fact, a modification of the GPISAR algorithm developed under the AFOSR contract for the synthetic focusing of laboratory GPR data (see the examples of GPISAR described in section 3.3 of this report and shown in Figures 3.3.2 and 3.3.3).

Figure 5.2.3 shows an unfocused C-scan image from one of the rocket motor sections at a depth range of 7-9" using the original algorithm developed by the customer. Notice the very complex interference artifacts and variety of shapes in the image. An unequivocal determination that there are no foreign objects present in the fuel cannot be made using Figure 5.2.3.

Figure 5.2.4 shows the same region imaged using the TSI focused, synthetic aperture, algorithm. This much higher resolution, interference artifact free image clearly shows that all the scattering objects are air voids - easily discriminated by their circular shape.

Figures 5.2.5 and 5.2.6 compare the focused and TSI focused images at a shallow depth range of 0.5 to 3". For shallow depth imaging a different scanner fixture employing a single 3/8" diameter transducer operating in pulse-echo mode at 500 KHz was employed. As in the deep scan case, the focused TSI algorithm provides a much higher resolution image of the scatterers, allowing the suspicious regions in the original unfocused C-scan image to be rejected as possible foreign objects.

Thus far, 3 rocket motor sections have been passed for flight, representing a savings of $15M to the customer. The spectacular success of TSI's solution to this NDT problem has prompted the customer company to begin contract negotiations with TSI for collaboration on the composite NDT problem described in section 7.7.2 below.

6.   Final Conclusions

Contributions and areas for commercial application.

Some of TSI's original goals for this project were not achieved. This was due mostly to the limited laboratory equipment available and a limited AFOSR budget that did not allow for extensive modifications to the laboratory scanner. In particular, it became evident that the original TSI x-y translation scanner and soil box were too small (6' by 4' and 16" deep for the sand box) to obtain the large aperture scattering data needed to image complex 2D objects. Also, since the antennas used were air-coupled horn antennas hovering above the surface of the sand

box, Snell's law limited the effective scattering aperture to $\pm 30°$ for buried targets, severely restricting the lateral (direction normal to depth for 2D) resolution of the system. This, coupled with large signal reflection losses at the air-sand interface and clutter signals form the scanner frame and sand box sides and bottom, made the imaging of general 2D objects unworkable. TSI's original goal of a 3D reconstruction of a complex target in the laboratory was not achieved. TSI's best inverse scattering reconstruction is of a circular cylinder buried in the sand and imaged with a circular symmetry constraint (which effectively fills out the missing lateral scan data).

Nonetheless, we believe that the theoretical advances, the software written, the simulations completed and the practical laboratory demonstrations, provided by this research contract, taken together as a whole, constitute a remarkable, significant and valuable contribution to basic science, to engineering know-how and to technology. This body of new knowledge has the potential for application to many commercial areas.

Some specific contributions and advances:

1. A theoretical model for inverse scattering that includes all orders of multiple scattering, that accurately predicts scattering with an error of a few percent or less and is fast enough to solve practical problems.
2. A robust, accurate inversion algorithm based on the theoretical model. This algorithm is not a perturbation or first order approximation (again it includes all orders of scattering) such as the Born or Rytov approximation. The use of multiple scattering provides the following advantages:
   a. Improved lateral spatial resolutions by a factor of 2 to 10 over conventional GPR.
   b. Improved depth spatial resolution by about a factor of 2

      c. Improved signal to noise and reduction of scattering artifacts

      d. Quantitative imaging of refractive index.

3. The implementation of the algorithm in optimized FORTRAN that can run on almost any computer (it is running on Macintosh, Pentium and Pentium-III, and UNIX computers such as the Sun Spark work station.

4. The construction of system simulation (models the most important features of a system) and emulation (a more accurate level of simulation that essentially models all of the features of a system) software. This enables the prediction of performance of scanning hardware before it is constructed. It is also the core of the inversion software (called the *forward* or *direct* model).

5. The construction of hardware to collect data for GPR modeling. The several scanners we have constructed are described in this report. They have produced images that demonstrate and validate the predictions of theory, simulation studies and the claims made above in item 2.

6. The use of the theory, algorithms and software in non-GPR applications. These include medical imaging, NDT of solid propulsion rocked motors, geophysical/geotechnical imaging, and SONAR imaging. The geotechnical work we have done imaging has potential for low frequency electromagnetic imaging of geological structures such as buried ordnance, and imaging buried liquid and solid waste.

Areas of application:

1. Finding buried mines and ordnance on land and in the ocean.

2. Finding buried liquid and solid waste.

3. NDT (see discussion of finding flaws in solid propellant rocket motors, which follows in the next section).

4. Medical imaging, in particular breast cancer screening and diagnosis. There is consderable synergy between the various imaging applications and algorithms. Inverse scattering for clinical imaging of the breast for cancer screening and diagnosis is one such important application of this synergy. TechniScan has been a leader in developing both: (1) single-step, linear, reflectivity backprojection imaging methods; and (2) iterative, non linear, transmission backpropagation (inverse scattering) imaging methods for medical imaging of breast cancer. Figure 6.1 and 6.2 show the significant progress made in improving spatial resolution of inverse scattering methods for breast cancer detection. In these figures, it is shown that 0.6 mm spatial resolution can be achieved at 5 MHz.

5. Evaluating roadbeds and bridge decks (see UDOT concrete and road imaging proposal, which follows in the next section).

7. Recommendations for Further Research

TSI is currently pursuing funding for the following three research projects to continue and extend the technology developed with the AFSOR contract:

7.1 DOE proposal summary:

TSI has concluded that further development of ISGPR will require a larger apparatus (to give a large aperture) and broad band, earth-coupled antennas that are placed in direct contact with the soil (to avoid the Snell's law limitation). The cost to have such antennas designed and built is in excess of $100K. Since full scale field antennas (100 MHz to 3 GHz) which are already available cost about the same price, TSI has concluded that the next logical step is to procure funding to build a full scale field system which would initially be calibrated and tested in a large, environmentally controlled soil pit (located in a warehouse, for example). TSI is presently preparing a proposal to the DOE to construct this system. The theoretical, algorithmic and experimental results achieved during the performance of the AFOSR contract substantially advanced the understanding of ISGPR and have effectively paved the way for the DOE field system.

TSI is submitting a four year proposal to the Department of Energy to develop a computer controlled, x-y-z scanning, back projection imaging and inverse scattering imaging, narrow time pulse yet stepped frequency, ground penetrating radar system (GPR) for characterizing sits containing buried waste. The system is designed to penetrate to depths of 6 to 20 feet and uses ground coupled antennas with a bandwidth of 20 MHz to 3 GHz. This system would incorporate all of the ground penetrating radar advances TSI has made including theory, algorithms

and hardware. TSI has three partners in the proposal: (1) Lintek, Inc. of Powell, Ohio would build the radar hardware; (2) Ohio State University would build the wide band, ground coupled antennas; and (3) MSI of Salt Lake City, UT and Denver, CO would supply the x-y-z linear motion and rotation components. TSI would integrate these components a motion control computer and software and with a DEC Alpha based workstation for imaging. The system would be portable to allow it to be taken to DOE sites or other sites and assembled for scanning...The system is not designed for surveillance of large areas (as are some GPR systems), but rather to provide accurate imaging of selected sites where other GPR systems do not have the sensitivity, spatial resolution, and image quality to be useful. If the operating frequency band were shifted up to 400 MHz to 20 GHz, the system would be useful for Humanitarian Demining operations for shallow antipersonnel mines in sites where extensive human traffic is present (trails, villages, farming plots, etc.). This research would be used by: (1) George Schneider, Ph.D. at DOE's Idaho National Engineering Laboratory, Idaho Falls, Idaho; (2) Brian Mathis, Director, D&D Technologies, CH2M HILL, Richland, WA; (3) Owen C. Robertson, Senior Project Manager, Remedial Action Project, Department of Energy, Richard Operations Office, Richland, WA.; and (4) Richard E. Smitherman, Col., USAF, BSC, Director, Environics Directorate, Armstrong Laboratory, Tyndall Air Force Base, FL.

The strategy for the direct application area will be to build a field-usable, ground penetrating radar system. We have already written a proposal to the DOE with a budget of about $2,000,000 to construct this system. This system will comprised of: (1) two Ohio State University dielectric filled, super wide band (4.5 octaves) antennas in bistatic mode for ground coupling; (2) a Lintek high speed, hybrid pulse and stepped frequency radar transmitter; (3) a dual programmable rail positioning $(x_1, y_1\ z_1; x_2, y_2, z_2)$ system for precise movement of the two respective antennas; (4) Pentium data collection computer; (5) a high speed parallel computer cluster for inversion; and (6) our inversion algorithms. We have contacts in the environmental remediation group at the DOE's Idaho National Engineering and Environmental Laboratory (INEEL) near Idaho Falls, ID. They have a need for this inverse tomography radar system to find buried utility lines (pipes, sewer, chemical lines, electric power, etc.) at a closed down plutonium processing plant and for imaging buried waste in pits. We also have contacts at the DOE's Richland, Washington, facility that have similar buried waste imaging needs. We have letters of commitment from these two DOE sites that state their need for this technology. The size of this market is at least $20 million over the next 5 years at DOE sites alone. As the value of the new radar is understood the market will increase to over $6 million per year in the next 5 years.

7.2 Composite Defect Imaging

TSI has been asked by the rocket motor manufacturer that funded the work in section 5.2 above, to participate in a research project to develop an imaging system to detect "wrinkles" in graphite fiber/epoxy composite rocket motor casings. TSI will be investigating both acoustic and EM methods in simulation and with laboratory data.

7.3 Utah Department of Transportation (UDOT) concrete imaging proposal

The main goal of this research effort will be to determine the applicability of using scattered energy in the form of microwave and/or ultrasonic energy (and associated imaging methods) for evaluation and monitoring of rebar integrity in concrete. TechniScan has developed a number of algorithms for imaging metallic and dielectric objects and has demonstrated these methods using data collected with a laboratory scale radar system for objects buried in sand. The system employs a HP-8720 network analyzer as the radar source and receiver. The antennas are two extremely broad band (1-18 GHz) ridged horns attached to two, independent x-y translation stages. The entire system is computer controlled. Simple modifications of this system will allow for scanning of concrete slabs in the laboratory and in the field. TechniScan has also developed ultrasonic and acoustic methods to imaging the human body (ultrasound) and objects buried in the soil (seismic). Each has advantages and optimal application areas. Each has disadvantages (microwave cannot penetrate electrically conducting materials, while acoustic methods cannot penetrate material with high air content or porosity. TSI has obtained UDOT approval to scan a set of bridge deck sections that are located in the University of Utah, civil engineering department. This will be done in the next few months. These results will then be used to support a more ambitious proposal to UDOT.

8.   Personnel

Principal Investigator:
David T. Borup
Executive Research Engineer
Ph.D., Electrical Engineering, University of Utah, Salt Lake City, Utah, 1989
Dissertation title: Fast-Fourier-transform based iteration methods for solving the electric field integral equation for anatomically based man models

Steven A. Johnson
TechniScan Chairman
Ph.D., Physics, Stanford University, Stanford, California, 1971
M.S., Physics, Stanford University, Stanford, California, 1967
Dissertation title: Photoelectronic storage spectroscopy, excited state absorption of chromium ion

James W. Wiskin
Research Mathematician
Ph.D., Mathematics, University of Utah, Salt Lake City, Utah, 1991
M.Sc., Mathematics, Dalhousie University, Halifax Nova Scotia, 1980
Dissertation title: Geometric and integral equation methods in scattering in layered media

Michael J. Berggren
Research Assoc. Professor, Bioengineering Dept.
Ph.D., Physics, Stanford University, Stanford, California, 1969
Dissertation title: Microwave Optical Investigations of Cr^{3+} Pairs in Ruby

9. Figures
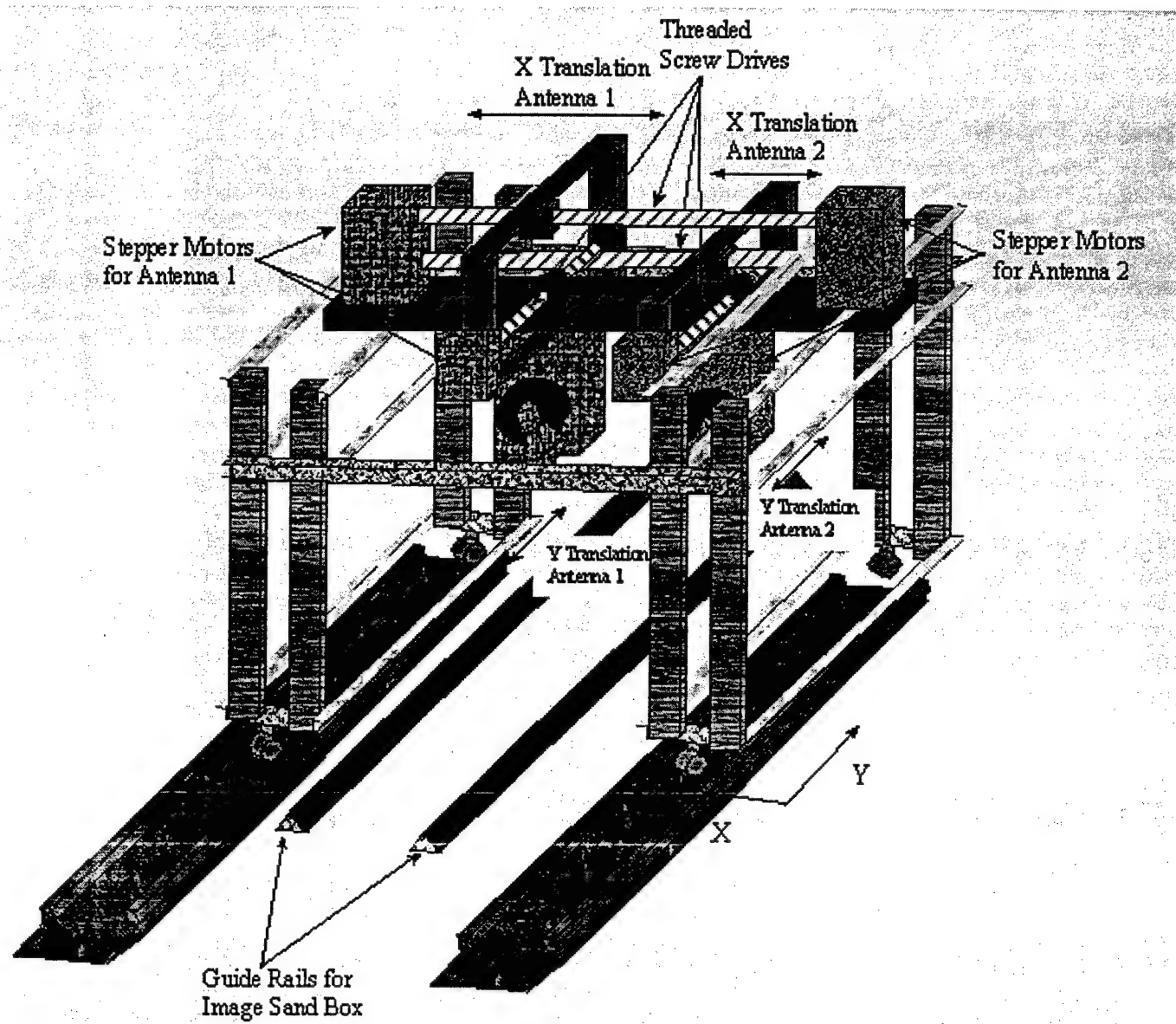
Figure 3.1.1 Diagram of the x-y translation scanner.
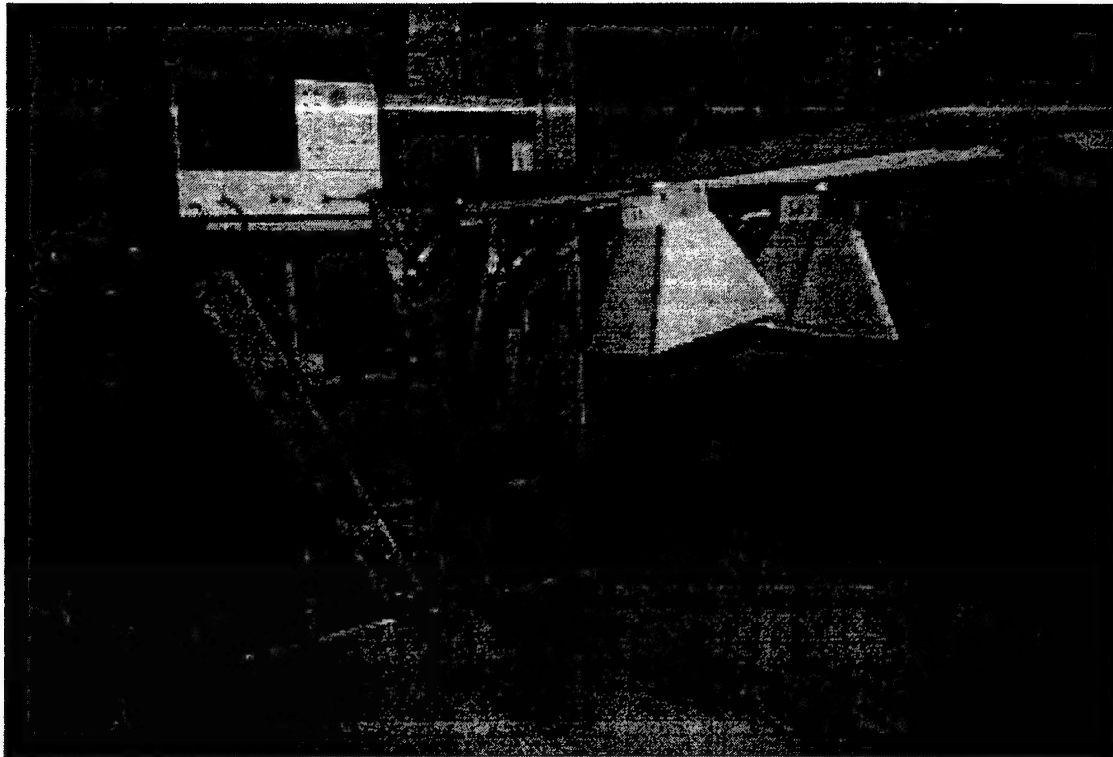
Figure 3.2.1 Photograph of the goneometer showing the rotation arms and antennas.

1-18 GHz
horn antennas

10°

77 cm

1" drywall

2" polystyrene foam

sand

15.5"
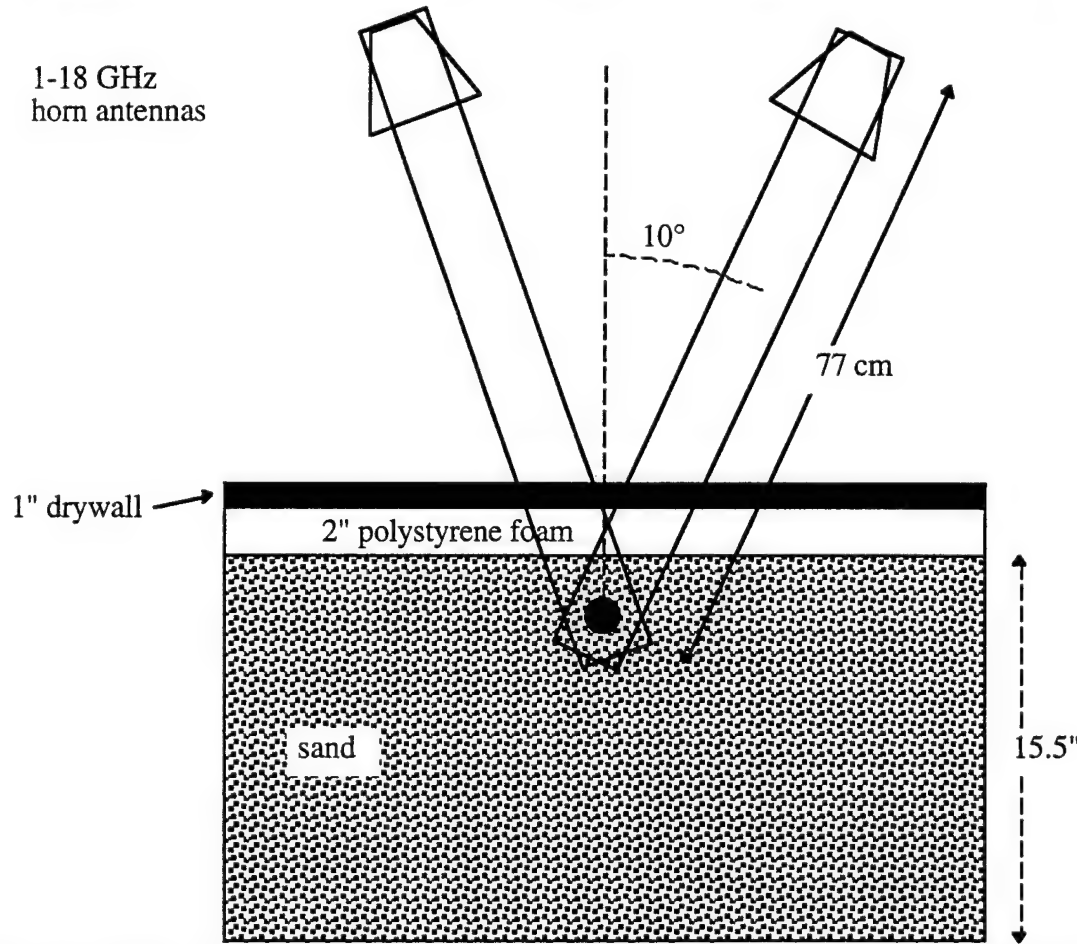
Figure 3.2.2 Geometry of the goneometer setup for imaging a drywall-polystyrene-sand model.
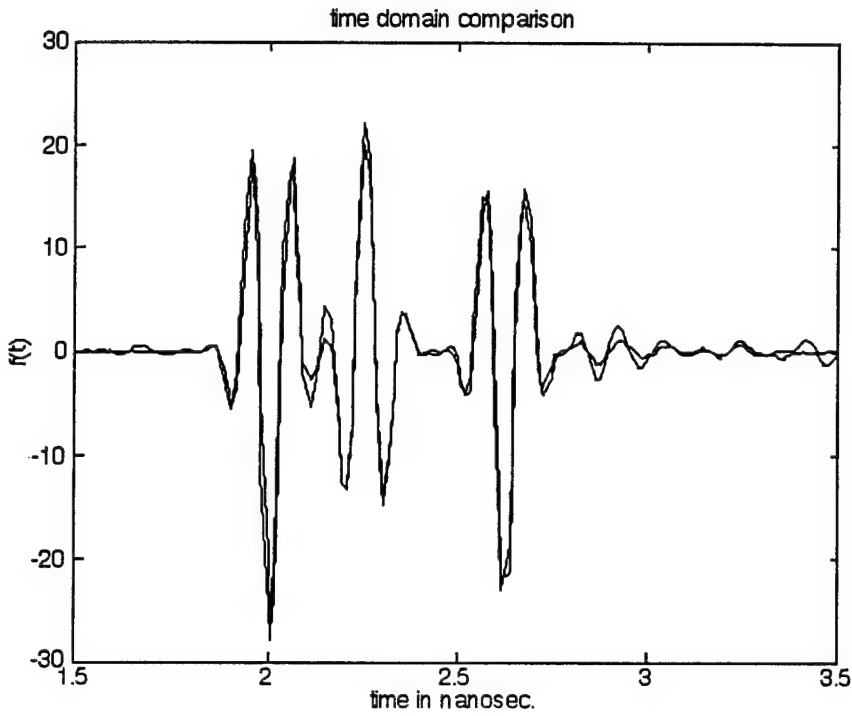
Figure 3.2.3 Time domain comparison of the goneometer data (blue) with data predicted from 1-D theory (red).
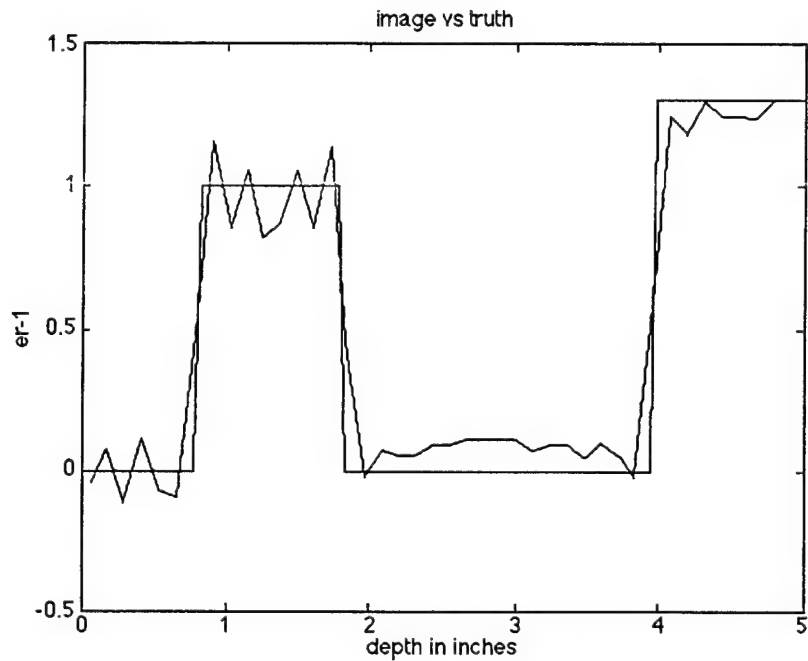
Figure 3.2.4 Comparison of the reconstructed (blue) and exact (red) $\varepsilon_r - 1$. The drywall begins at x = 0.8" and the sand interface begins at x = 4".
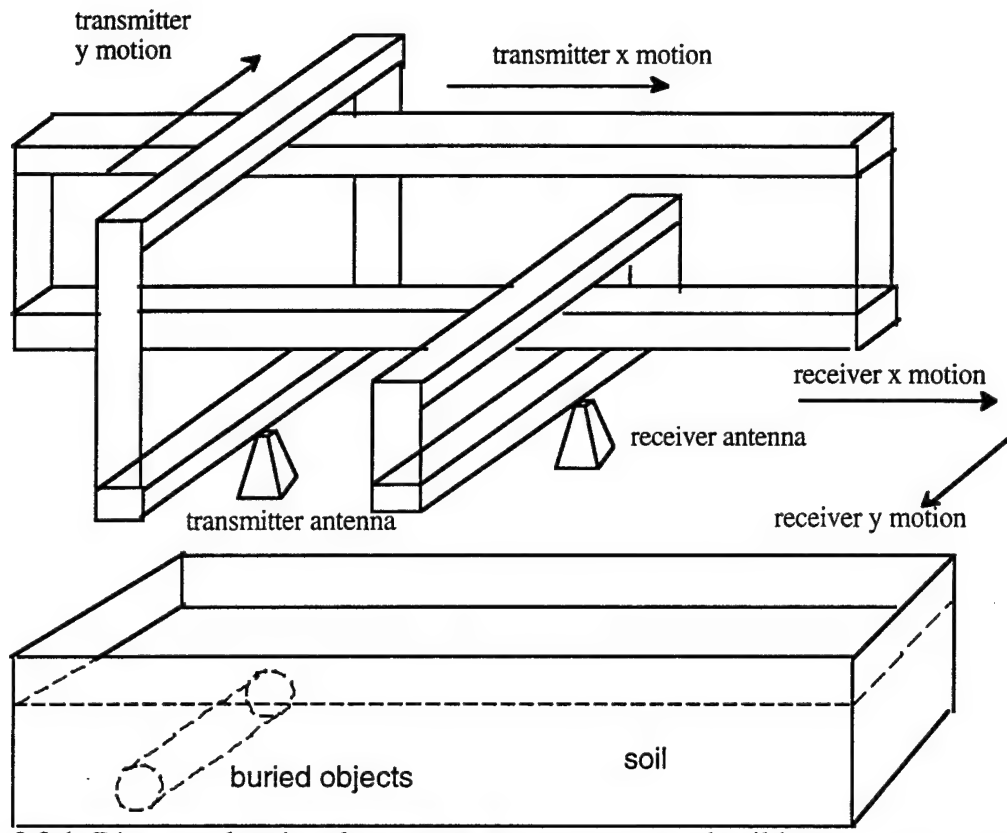
Figure 3.3.1 Diagram showing the x-y scanner geometry and soil box.
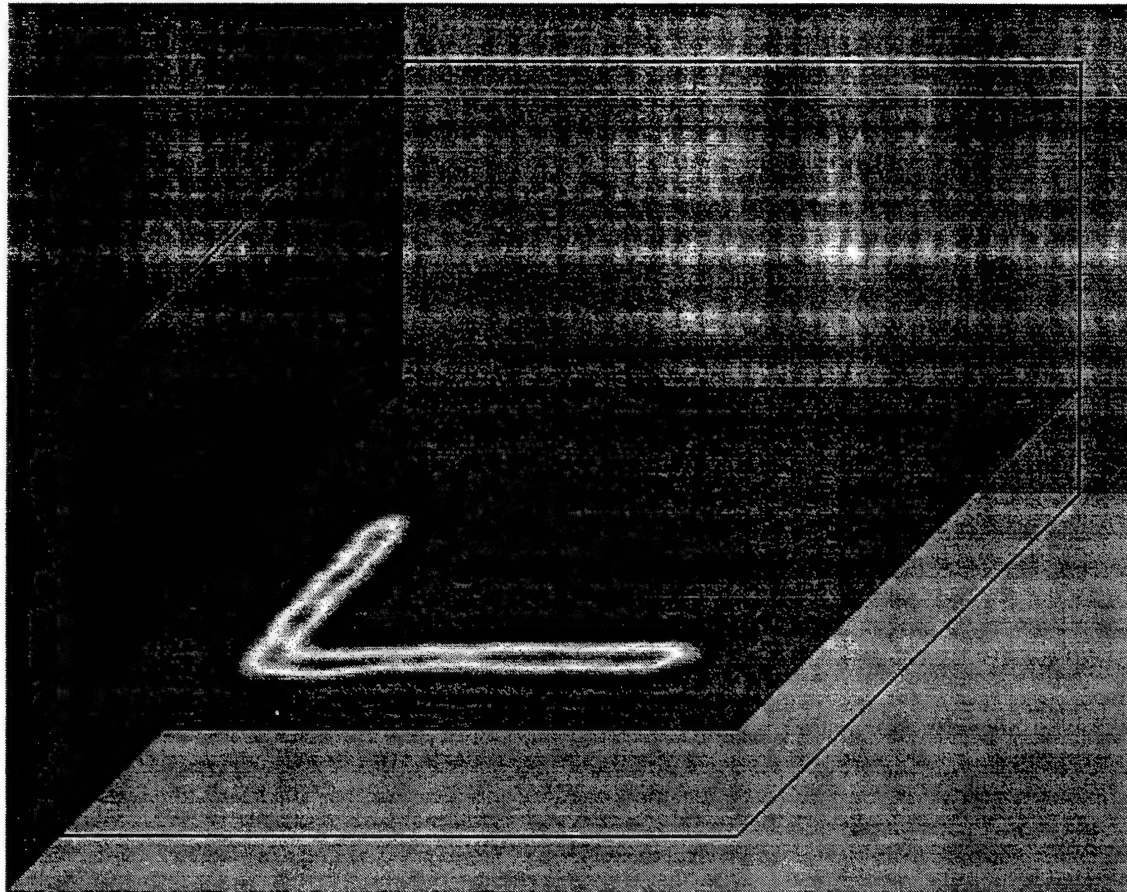
Figure 3.3.2 GPISAR image of the carpenters square buried in the sand. The image space is 64 by 64 by 40 cm (x,y,z).
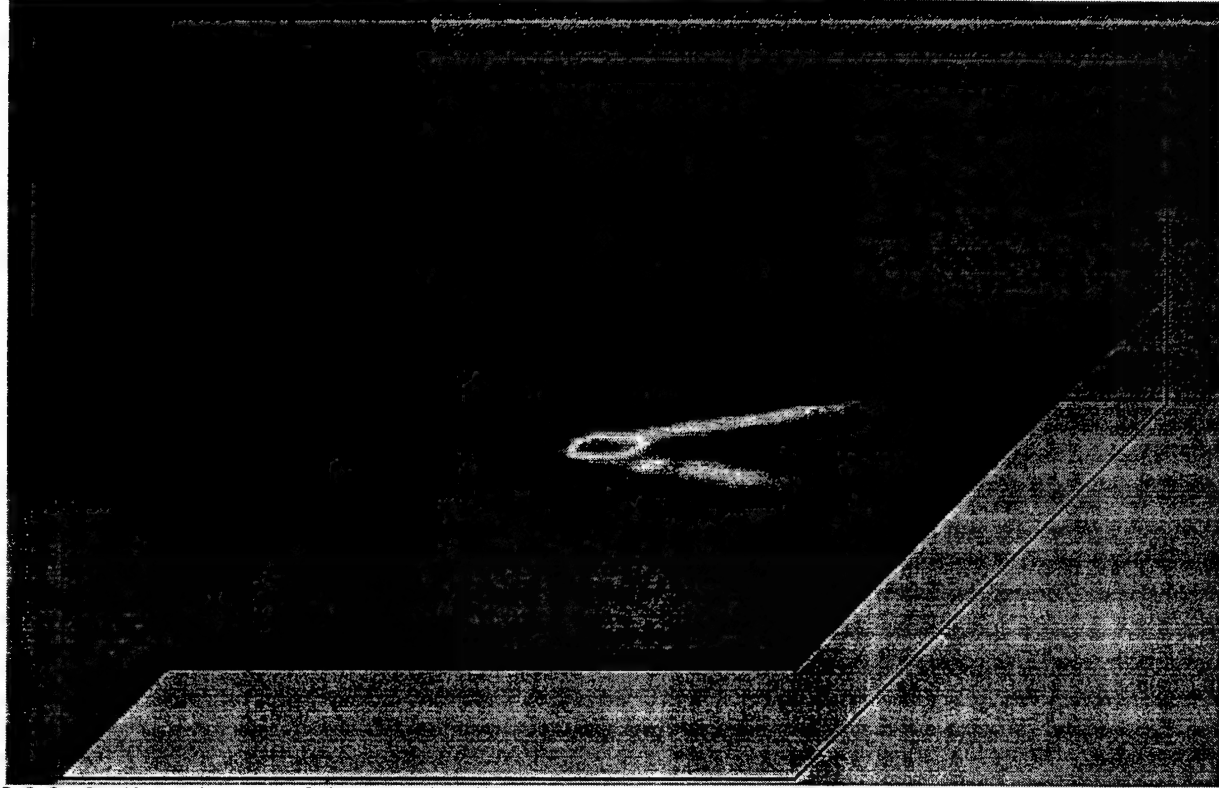
Figure 3.3.3 GPISAR image of the metal caliper buried in the sand. The image space is 70 by 70 by 32 cm (x,y,z).

time domain comparison
solid=exact, dashed=data
0.5 to 17 GHz cosine window
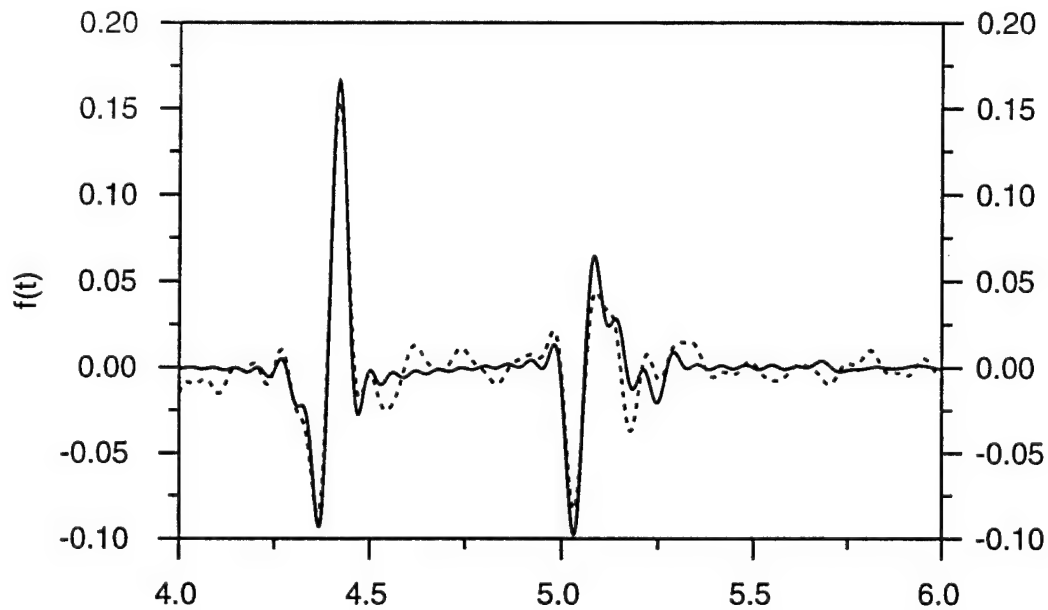
Column1

Figure 3.3.1 Comparison of the time domain scattering from the 4", air-filled PVC pipe. The solid line is the theoretical prediction (exact solution for the 2-D TM case) and the dashed line is the laboratory data. The horizontal axis is time in nanosec.
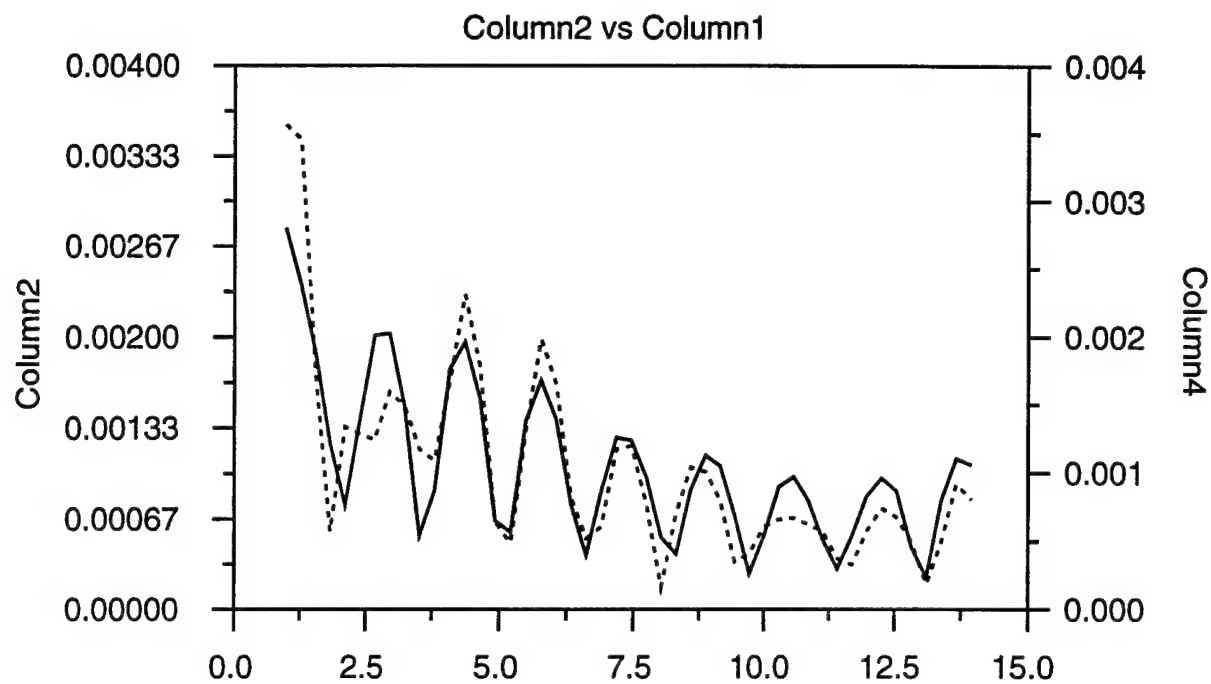
Column2 vs Column1

Figure 3.3.2 Frequency comparison of the modulus of the exact solution (solid line) and the laboratory data (dashed line) for the 4" dia., air-filled PVC pipe. The horizontal axis is the frequency in GHz.

Column2 vs Column1
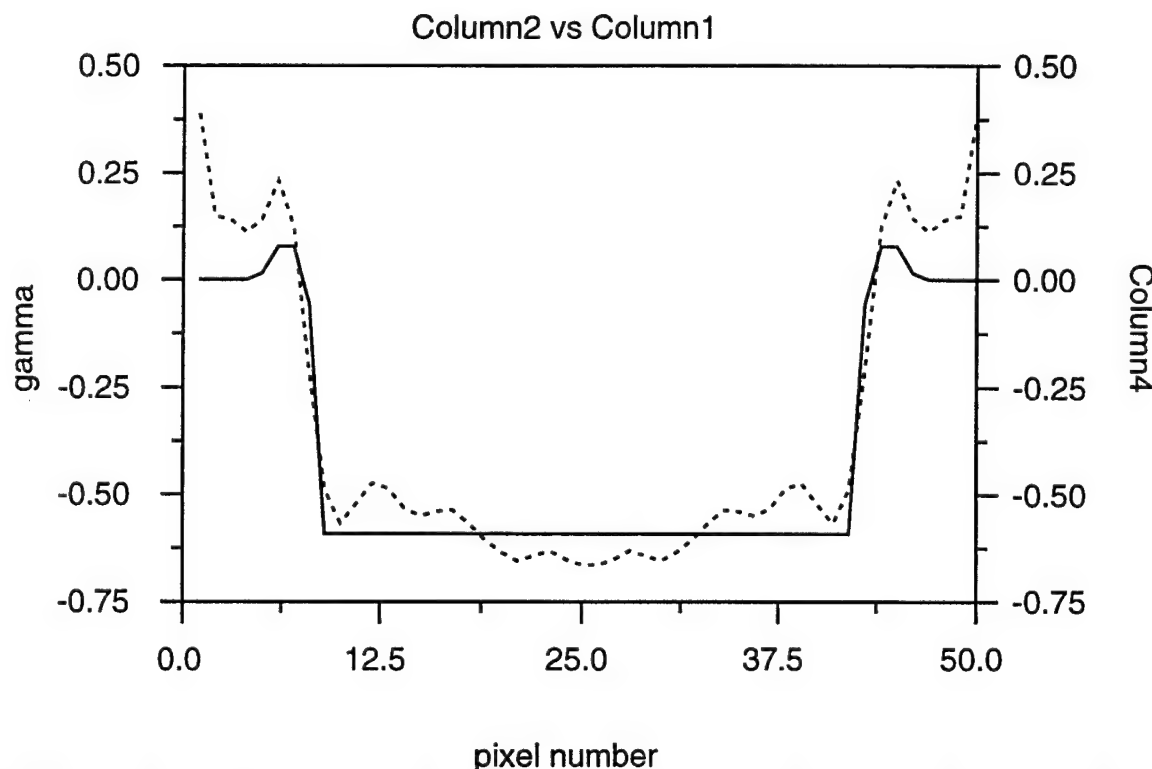
Figure 3.3.3 Comparison of the reconstruction (dashed) with the true dielectric distribution (solid) on an axis through the center of the pipe. Plotted is the scattering potential relative to the sand:
$$\text{gamma}(x,y) = \varepsilon_r(x,y)/\varepsilon_r(\text{sand}) - 1.$$
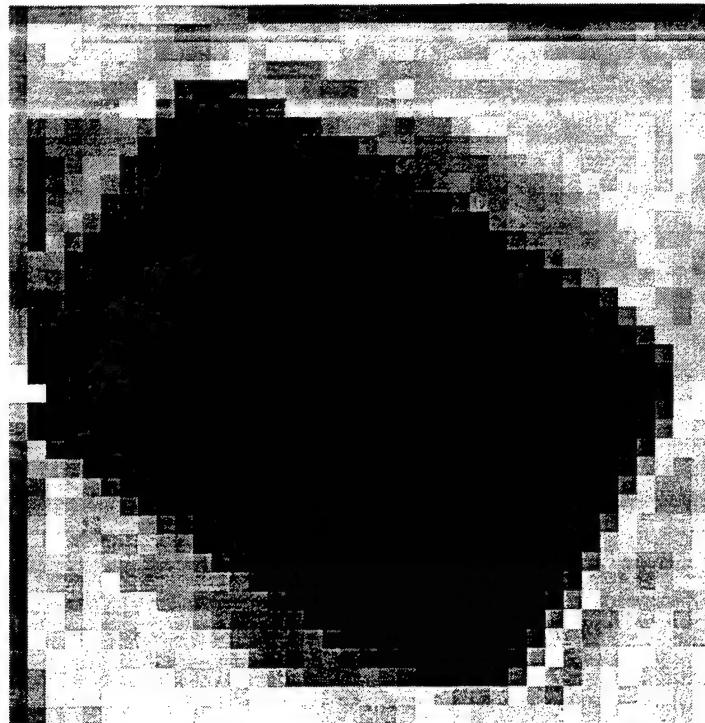
Fig. 3.4.3.1 Early TechniScan EM tomographic image of a wooden block. The image is 20 by 20 cm. The block is 6 by 4 inches.
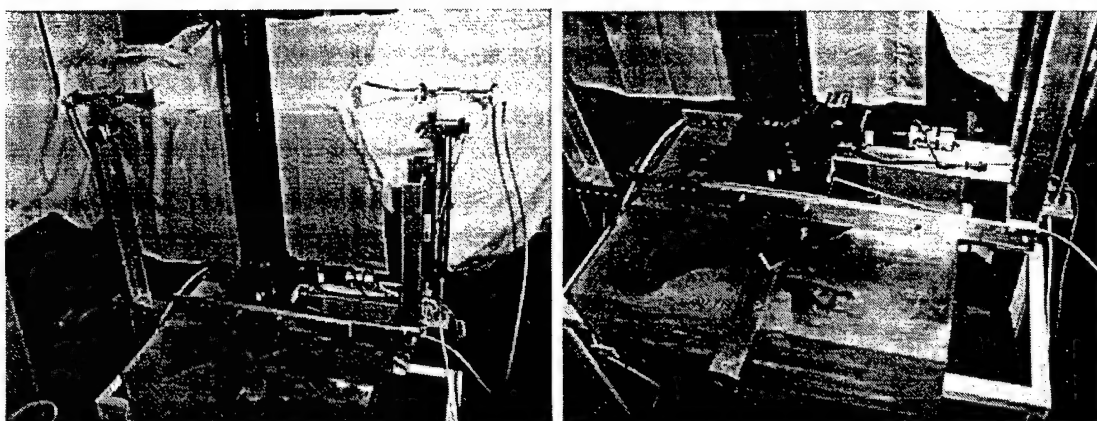
Fig. 3.4.3.2: Photographs of TechniScan's microwave tomographic scanner.
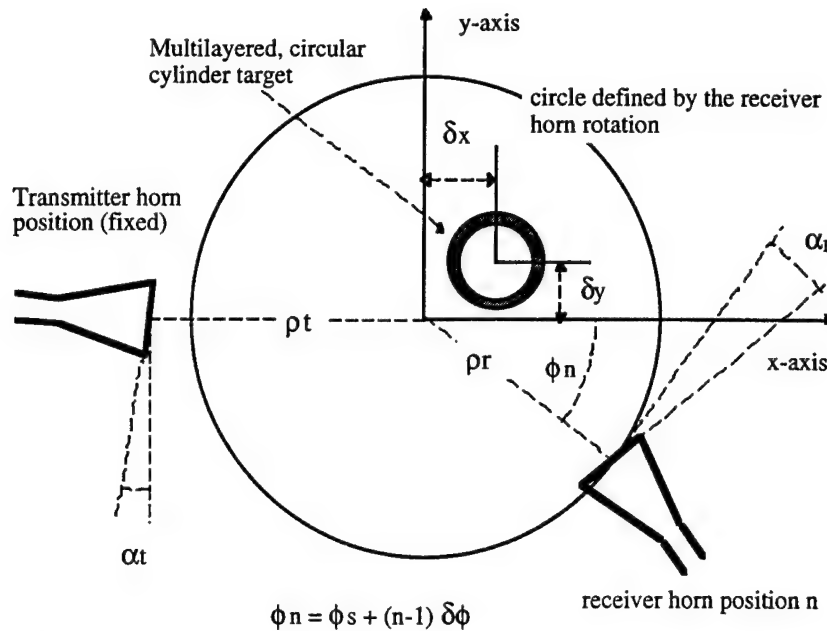
Fig. 3.4.3.3. Illustration of the calibration parameters determined by the calibration algorithm for a single view of a cylindrically symmetric target.
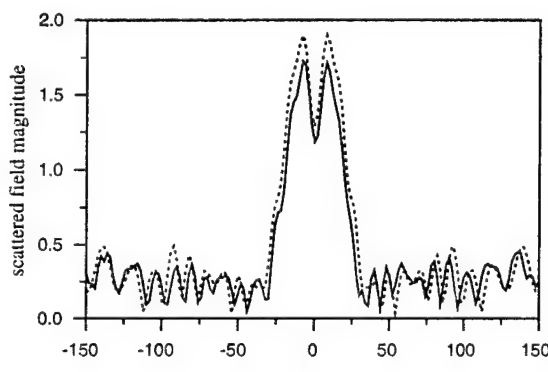
Fig. 3.4.3.4
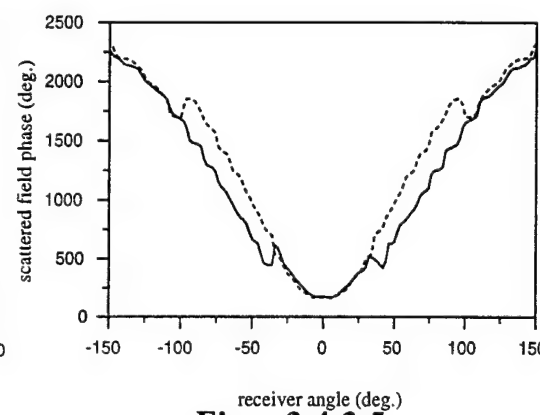
Fig. 3.4.3.5

Lab data scattered field magnitude(Fig. 3.4.3.4) and phase (Fig 3.4.3.5) (solid) and the uncalibrated theoretical prediction (dashed)
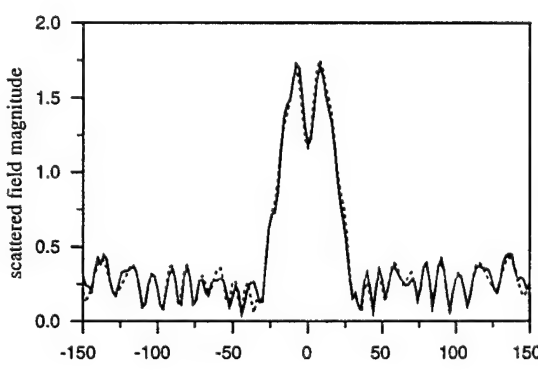
Fig. 3.4.3.6.
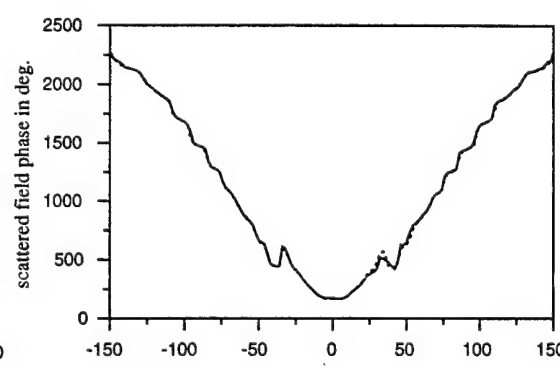
Fig. 3.4.3.7.

Lab data scattered field magnitude (Fig. 3.4.3.6) and phase (Fig. 3.4.3.7) (solid) and the optimized calibrated theoretical prediction (dashed)
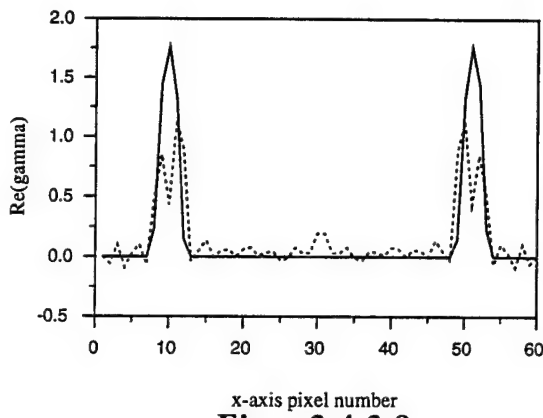
Fig. 3.4.3.8.
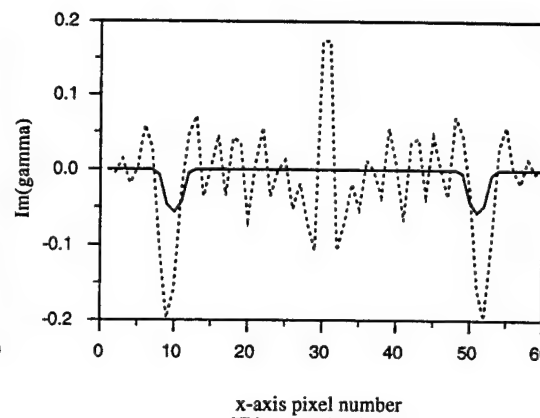
Fig. 3.4.3.9

Comparison of the true (solid) and reconstructed (dashed) γ for both the real (Fig. 3.4.3.8) and imaginary (Fig. 3.4.3.9) parts for our original algorithm without constraints.
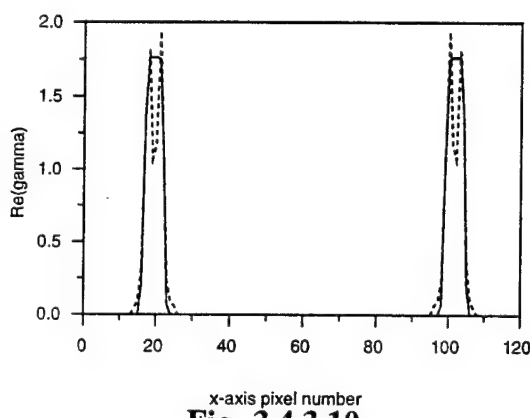
Fig. 3.4.3.10.
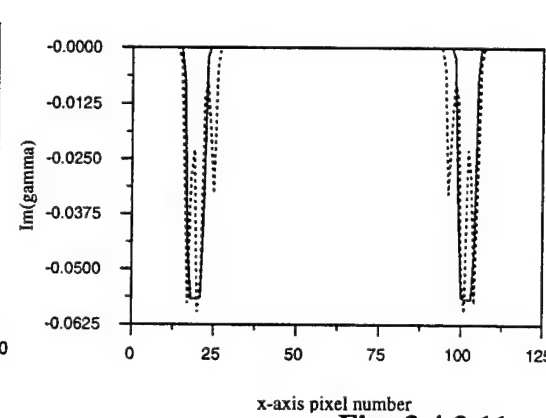
Fig. 3.4.3.11

Comparison of the true (solid) and reconstructed (dashed) γ for both the real (Fig. 3.4.3.10) and imaginary (Fig. 3.4.3.11) parts for our new algorithm employing the sign constraint.

Transducers scan a defect standard to validate system performance before and after each motor scan.
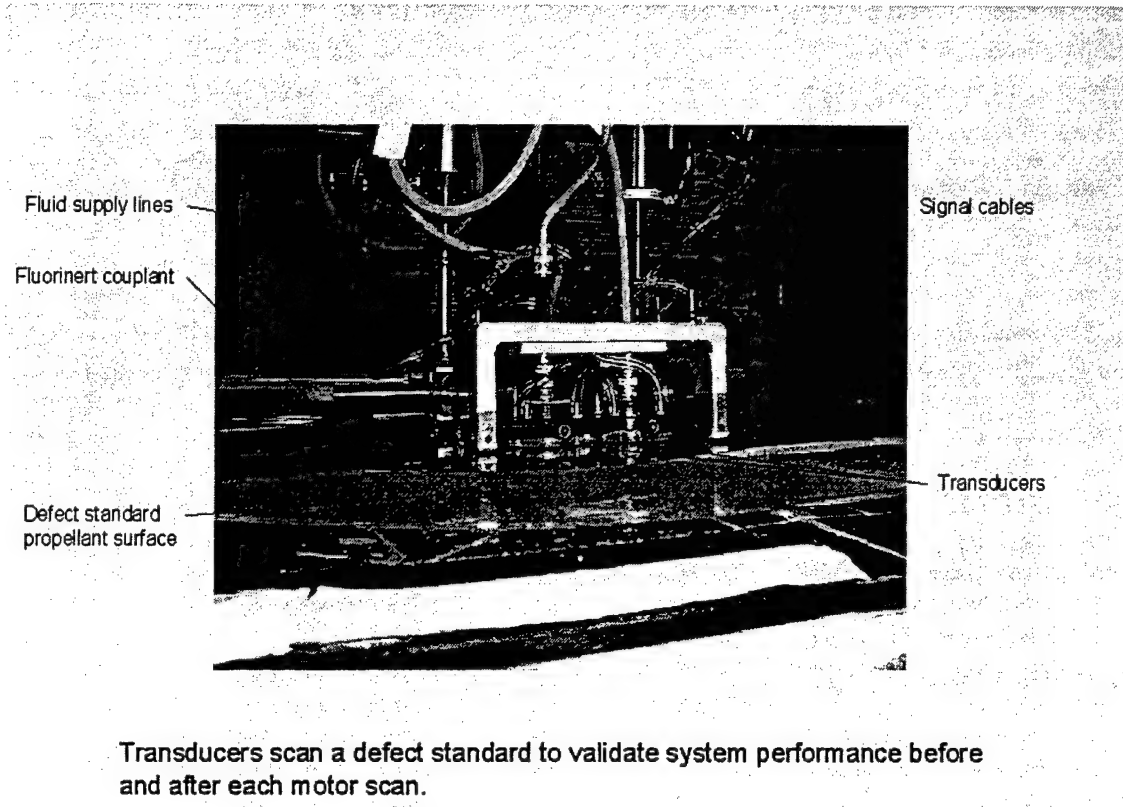
Figure 5.2.1 Photograph of scanning apparatus used to image fuel in solid fuel rocket motor.

Embedded Rubber Defect Standard (shallow depth)
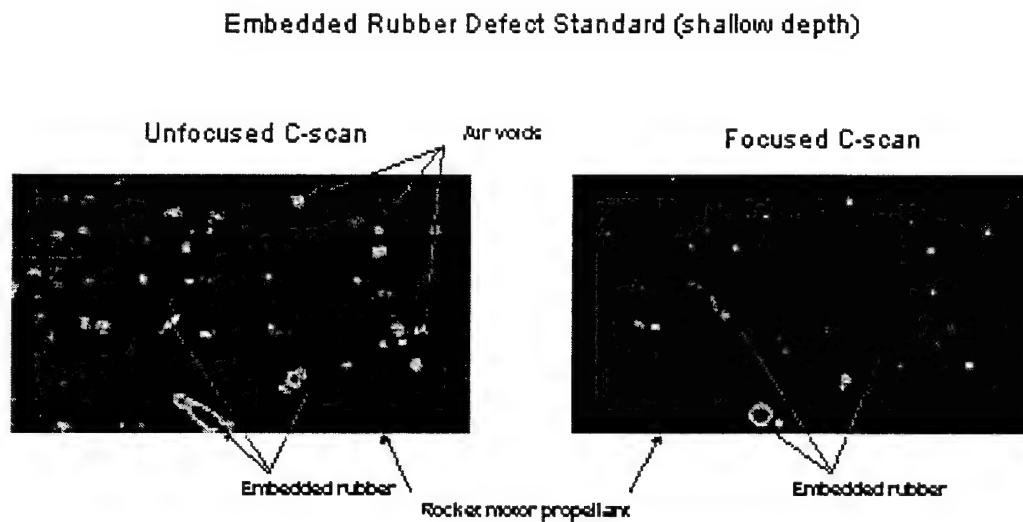
Synthetic aperture algorithm does extraordinary imaging of embedded material

Figure 5.2.2 The original image is in the left panel. The image focused by TechniScan is in the right panel.

Unfocused data - C-scan image (7-9" depth slice)
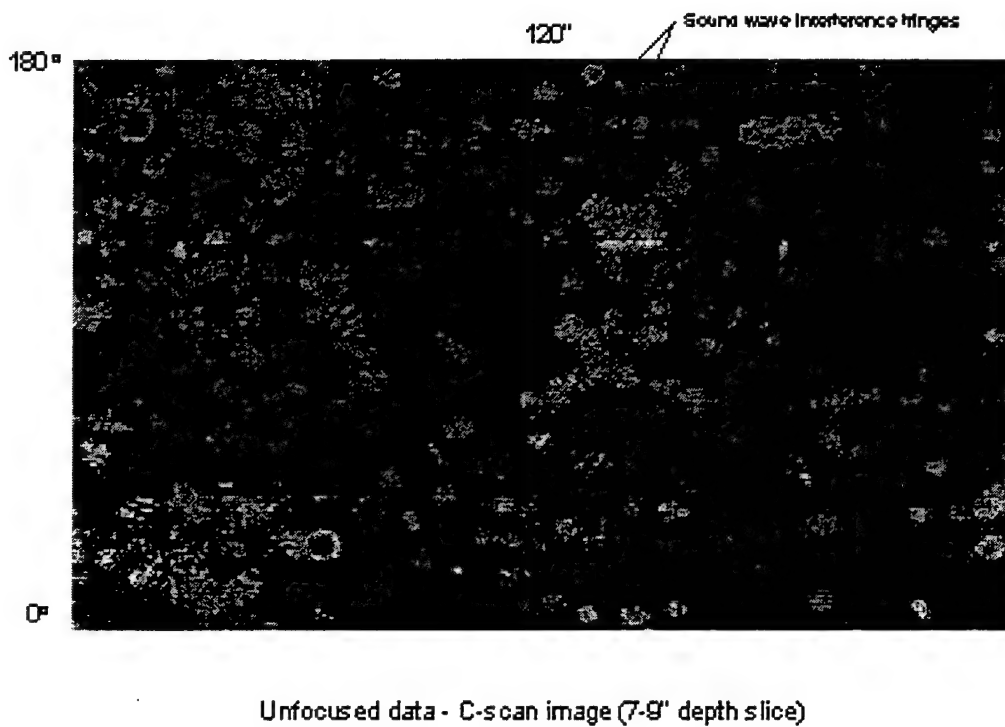
Figure 5.2.3 Image <u>before</u> application of TechniScan focusing algorithm.

Same data after applying focusing algorithm

Figure 5.2.4 Image <u>after</u> application of TechniScan focusing algorithm to same data.

Pulse Echo Scan Data - Depth Slice 2.1' to 2.9' (156 - 215)
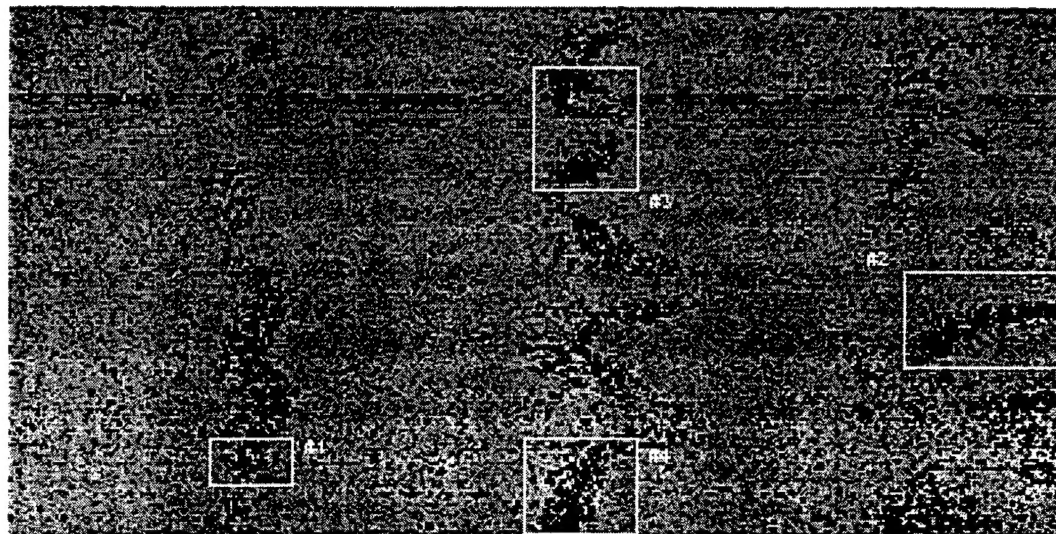
Propellant very non-homogeneous at several locations -
(could mask presence of embedded foreign material)

Figure 5.2.5 Shallow scan image <u>before</u> application of TechniScan focusing algorithm.

Depth Slice 0.5' to 3.0'
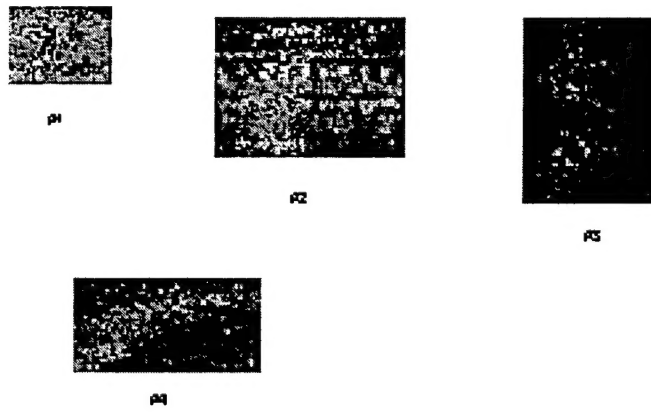
Same data (in boxed areas) after applying focusing algorithm

Figure 5.2.6 Shallow scan image <u>after</u> application of TechniScan focusing algorithm to same data.
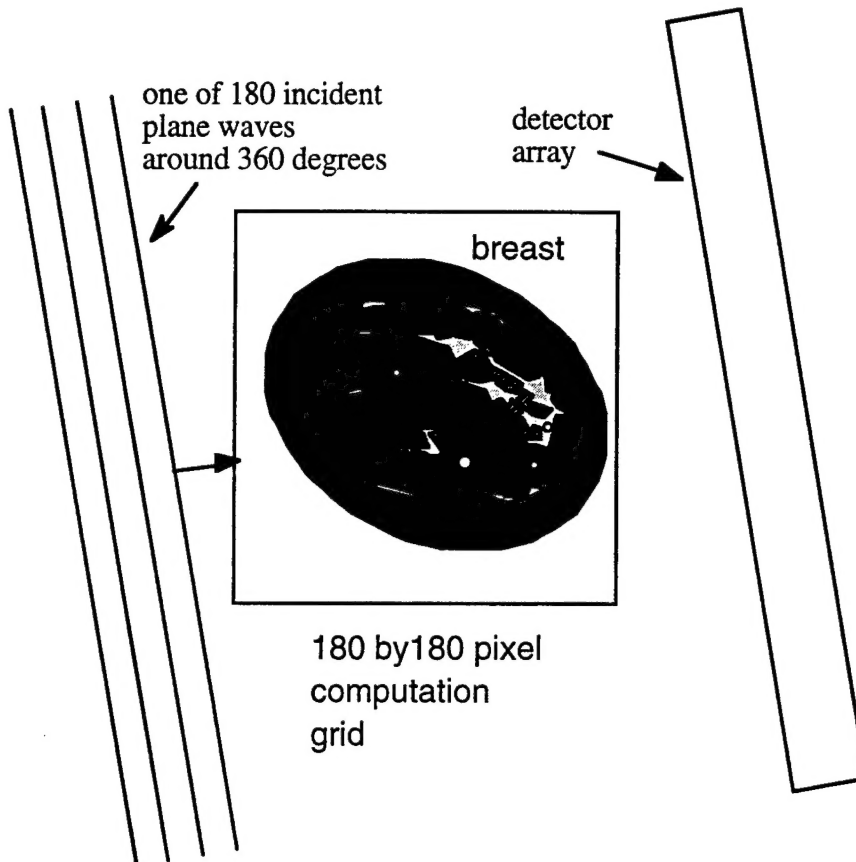
Figure 6.1

Ultrasound Inverse Scattering Imaging was acheived from ultrasound scattering data derived from an MRI (Magnetic Resonance Imaging) breast phantom. This result was made just recently (30 May 2000) and is important because we now have reached 5 MHz where the resulting tight vertical focusing is an added bonus. A water bath geometry was used. This same geormetry can be used for scanning patients in a commercial version.

Frequency = 5 MHz

Displayed Pixel dimension = λ at 5 MHz in water (1500 m/s) = 0.3 mm

Array size = 360 × 360 pixels = 4.25 × 4.25 inches
Number of plane wave views = 720

Linear receiver array = 720, λ length elements = 8.5 inches long

Object phase shift = $-6.8\ \pi$

Object attenuation = -11.8 dB
Run time = 2.5 hours.

TABLE 1 -- Tissue properties of the model:

|	
c_{water}=1500 m/s	α_{water} = 0.0 dB/cm/MHz
c_{fat} = 1458 m/s	α_{fat} = -0.41 dB/cm/MHz
$c_{glandular}$= 1540 m/s	$\alpha_{glandular}$ = -0.80 dB/cm/MHz
c_{tumor}= 1564 m/s	α_{tumor} = -1.18 dB/cm/MHz
c_{cyst}= 1568 m/s	α_{cyst} = -0.10 dB/cm/MHz
Total Across Object phase shift = $-3.4\ \pi$	Total Across Object attenuation = -5.9 dB
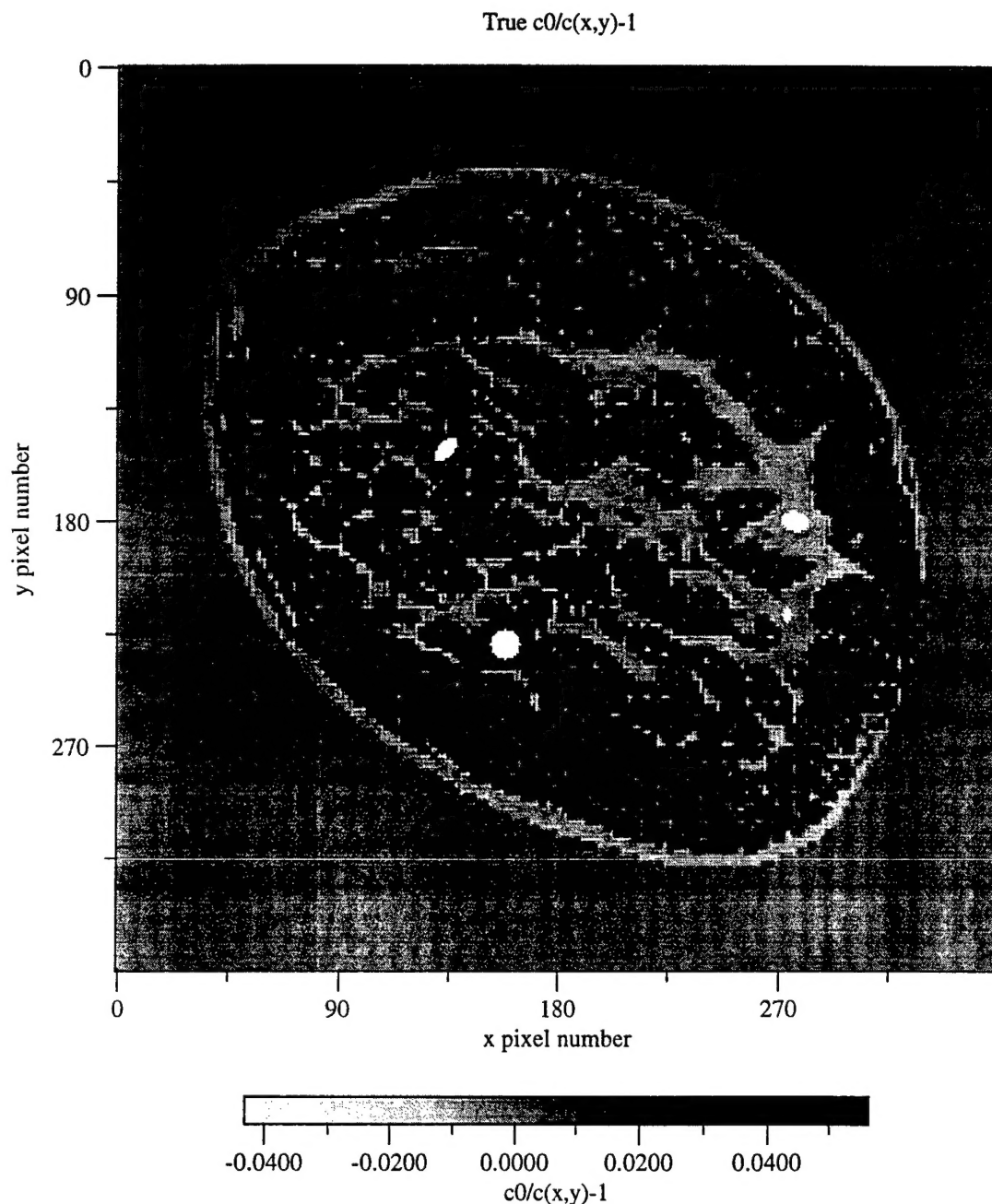
True c0/c(x,y)-1

Figure 6.2
Gray scale image of true version of $[c_0/c(x,y) - 1]$.

Inverse scattering reconstruction of c0/c(x,y)-1
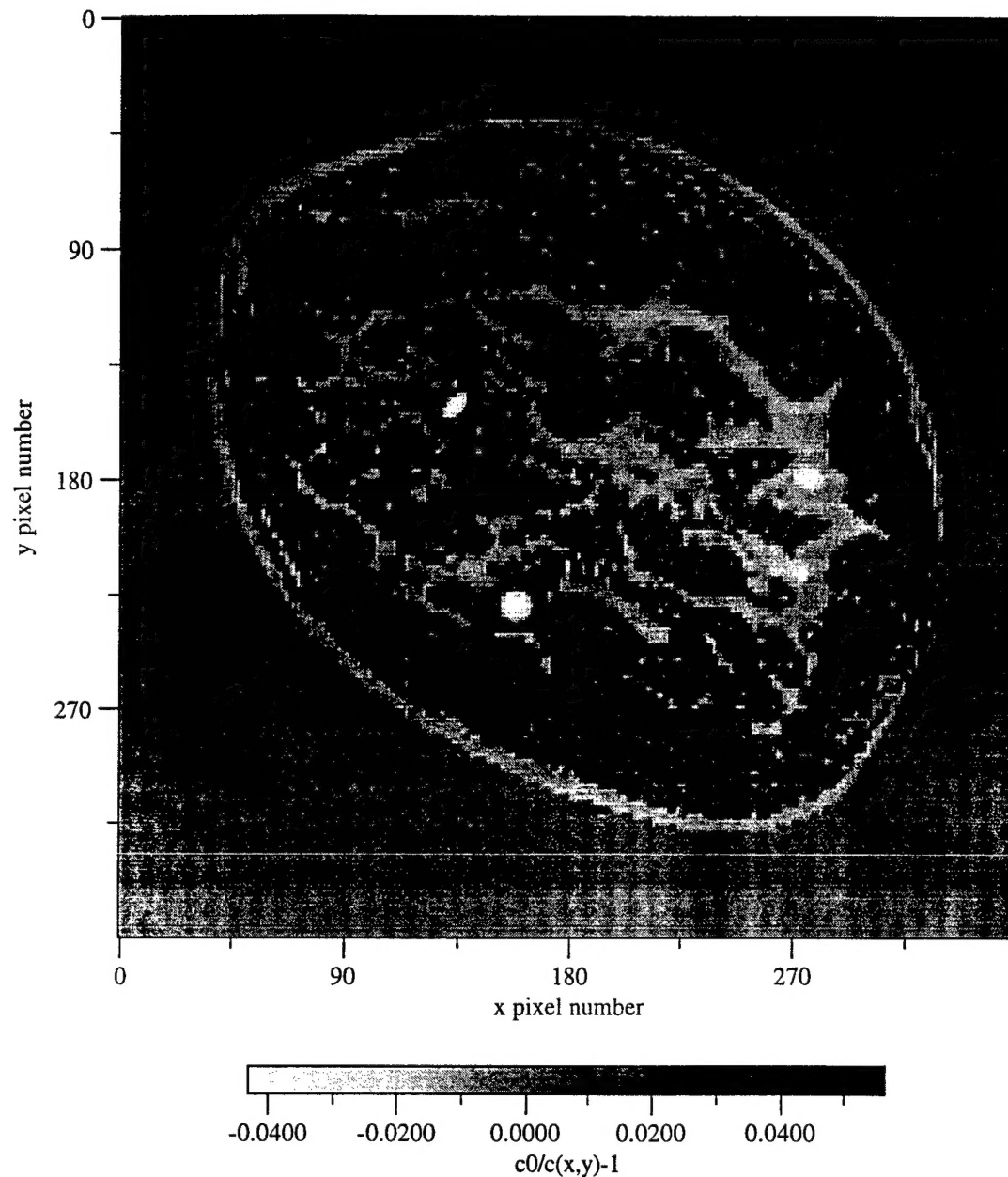
Figure 6.3

Gray scale image of the inverse scattering image of $[c_0/c(x,y) - 1]$.
Compare this with the true version or test object that represents a true cross
section of speed of sound $c(x,y)$. From the scattering data the reconsructed
version will be made by inverse scattering.